

USGS Award No. G12AP20083

**PROBABILISTIC SEISMIC LANDSLIDE MAPS:
IMPLEMENTATION PROJECT**

FINAL TECHNICAL REPORT

SUBMITTED: June 2014

ELLEN M. RATHJE, PH.D., P.E.

University of Texas at Austin
ECJ 9.227C, C1792
Austin, TX 78712
Tel: 512-232-3683
Fax: 512-471-6548
e.rathje@mail.utexas.edu

AWARD PERIOD

June 2012-January 2014

Research supported by the U.S. Geological Survey (USGS), Department of the Interior, under USGS award number (G12AP20083). The views and conclusions contained in this document are those of the authors and should not be interpreted as necessarily representing the official policies, either expressed or implied, of the U.S. Government

ABSTRACT

Current hazard mapping efforts for earthquake-induced landslides use sliding block displacements to evaluate the potential for earthquake-induced landslides. In these procedures, slopes that are predicted to develop significant downslope displacements during an earthquake are deemed seismically unstable. However, these procedures typically use a deterministic approach, in which the variability in the expected ground motion and the displacement prediction are ignored. Additionally, these procedures do not consider the epistemic uncertainty in the slope properties (i.e., soil shear strengths, ground water table location, and thickness of sliding blocks). Ignoring these variabilities and uncertainties can lead to poor estimates of the actual seismic landslide hazard.

A probabilistic approach to seismic landslide hazard mapping is described that accounts for the assorted variabilities and uncertainties inherent in the analysis. The approach uses a displacement hazard curve to account for the variability in the expected ground motion and the displacement prediction, and uses a logic-tree analysis to incorporate the epistemic uncertainties in the slope properties. This report describes the probabilistic approach to seismic landslide hazard mapping and the incorporation of a logic-tree analysis to account for various sources of epistemic uncertainties. An efficient computational scheme is described that allows the logic-tree approach to be applied more easily to regional analysis. The new probabilistic approach is used to develop a seismic landslide hazard map for Anchorage, Alaska.

The results show that including the effects of variability and epistemic uncertainties identifies the area of high/very high hazard that is 3 times larger than identified through the deterministic approach. The influence of the epistemic uncertainty in the sliding block properties is generally greater than the influence of the epistemic uncertainty in the shear strengths because the uncertainties in sliding block properties are larger than the uncertainties in shear strength. Comparison with a previous deterministic seismic landslide map developed by the USGS indicates that the seismic landslide hazard from the probabilistic analyses performed in this study is smaller because the deterministic map used very conservative assumptions with respect to the sliding block properties. This comparison indicates that the logic-tree approach provides an alternative way to rigorously account for uncertainties in slope properties, and it can avoid using overly conservative input parameters to capture these uncertainties in a deterministic approach.

1.0 INTRODUCTION

Seismic landslides have been responsible for a tremendous amount of economic losses in earthquakes. For instance, the 2008 Sichuan Earthquake ($M_w = 7.9$) in China induced significant landslides and these landslides not only buried dozens of towns, but also blocked roads, which are the lifelines connecting those ruined towns and nearby large cities. Knowledge of the locations and scale of potential seismic landslides is essential for reducing losses caused by earthquakes.

Regional maps of potential seismic landslides are used in land-use planning and emergency-response planning, and are used to identify zones that require detailed, site-specific studies. Current seismic landslide hazard mapping efforts utilize empirical predictions of sliding displacement based on the expected ground shaking and the general slope properties (e.g. Jibson et al. 2000). The seismic landslide hazard is assigned qualitatively as high, medium, or low based on the different displacement thresholds. However, these maps typically utilize a deterministic approach that does not consider the aleatory variability in predictions of ground shaking or sliding displacement; nor do they consider the epistemic uncertainty in the slope properties (i.e., soil shear strengths, ground water table and thickness of sliding blocks).

A recently developed probabilistic approach uses a sliding displacement hazard curve to quantify the seismic landslide hazard (Rathje and Saygili 2008). The displacement hazard curve incorporates aleatory variability to compute the annual frequency of exceedance (i.e., hazard) of different displacement levels, and it is used to identify the displacement associated with a specified hazard level (Saygili and Rathje 2009). Using the displacements associated with the specified hazard level (typically 10% or 2% probability of exceedance in 50 years), a seismic landslide hazard map is produced using the same displacement thresholds used in deterministic approaches. However, this probabilistic approach does not incorporate any epistemic uncertainty in the slope properties. Yet, at a regional scale the uncertainties in the slope properties are significant and should be taken into account.

This research uses a logic-tree analysis to incorporate the epistemic uncertainties in the slope properties into the probabilistic framework. This report describes the probabilistic approach to seismic landslide hazard mapping and the incorporation of a logic-tree analysis to account for various sources of epistemic uncertainties. An efficient computational scheme is described that allows the logic-tree approach to be applied more easily to regional analysis. The new probabilistic approach is used to develop a seismic landslide hazard map for Anchorage, Alaska.

2.0 SEISMIC LANDSLIDE HAZARD MAPPING

2.1 Sliding Block Displacement Analysis

During an earthquake, the soil mass on a slope experiences inertial forces due to the ground shaking. The seismic loading force can be represented by the mass of the soil (W/g) multiplied by a seismic coefficient (k), $F = k \cdot W/g$. The yield acceleration (k_y), or yield seismic coefficient, represents the seismic loading that initiates instability and is equal to the seismic coefficient that produces a factor of safety equal to 1.0.

In natural slopes, a common failure mode for seismic landslides is a thin, veneer slope failure (Keefer 2002). In this case, the depth of the failure surface (typically several meters) is much smaller than the length of the slope failure (dozens of meters to hundreds of meters) and an infinite slope model can be used to assess the stability of the slope. The infinite slope assumption commonly is used for seismic landslide hazard mapping to estimate k_y . Figure **Error! No text of specified style in document..1** shows an infinite slope model for static conditions. W is the weight of the failure block, σ and τ are the normal and shear stresses on the failure surface, c' is the effective cohesion, ϕ' is the effective friction angle, γ is the material unit weight, γ_w is the unit weight of water, α is the slope angle, t is the slope-normal thickness of the rigid block, and m is the proportion of the block thickness that is saturated and thus represents pore water pressure. The static factor of safety can be expressed as:

$$FS_{\text{static}} = \frac{c' + (\gamma - m \cdot \gamma_w) \cdot t \cos \alpha \cdot \tan \phi'}{\gamma \cdot t \cdot \sin \alpha} = \frac{c'}{\gamma \cdot t \cdot \sin \alpha} + \frac{\tan \phi'}{\tan \alpha} (1 - m \cdot \frac{\gamma_w}{\gamma}) \quad (\text{Error! No text of specified style in document..1})$$

Assuming ground shaking parallel to the slope, the yield acceleration that produces $FS_{\text{seismic}} = 1.0$ can be calculated as:

$$k_y = (FS_{\text{static}} - 1)g \cdot \sin \alpha \quad (\text{Error! No text of specified style in document..2})$$

where g is the acceleration of gravity. The ground shaking can also be assumed as horizontal, but in most cases the resulting yield acceleration only has a small difference (Saygili, 2008).

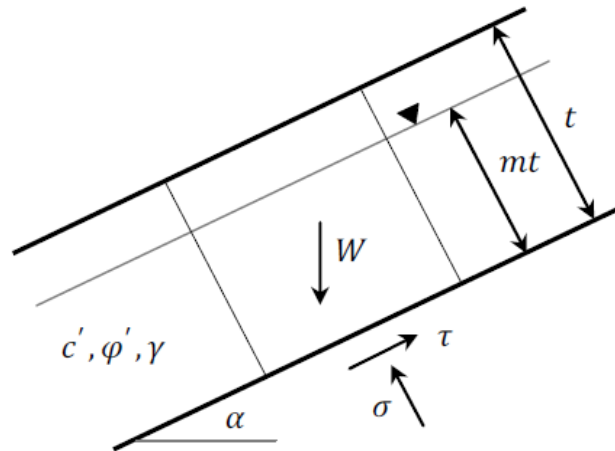


Figure Error! No text of specified style in document.1 Infinite Slope Model under Static Condition

Sliding block displacements are computed for a given yield acceleration (k_y) and earthquake ground motion (Newmark 1965). For rigid sliding block analysis, the slope is considered a rigid block sitting on a base (i.e. failure surface). Given an acceleration-time history, sliding starts when the acceleration-time history exceeds the yield acceleration and it continues until the relative velocity between the sliding block and base drops back to zero. Figure Error! No text of specified style in document.2 shows a schematic of the rigid sliding block analysis. At point X, where the ground acceleration reaches the level of the yield acceleration, sliding starts. The relative acceleration between the base and k_y is numerically integrated to obtain the relative velocity, and the relative velocity is numerically integrated to obtain the relative sliding displacement. At point Y, the ground acceleration decreases to the k_y level, but the sliding does not stop due to non-zero relative velocity. At point Z, the relative velocity becomes zero and sliding stops. Sliding is triggered each time the ground acceleration exceeds the k_y level. To calculate the relative displacement between the sliding block and base for the entire time history, the relative acceleration-time is integrated twice with respect to time in the ranges when sliding occurs.

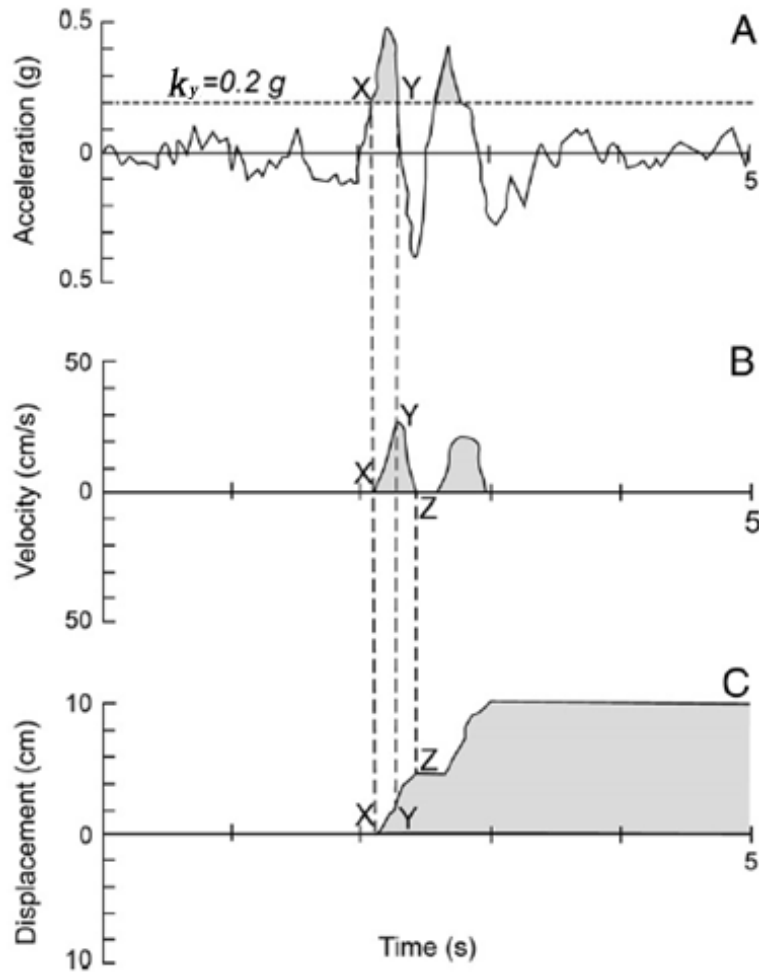


Figure **Error! No text of specified style in document..2** Illustration of rigid sliding block analysis (adapted from Wilson and Keefer 1983 by Jibson et al. 2000)

Instead of directly using acceleration-time histories to predict rigid sliding block displacements, many empirical models have been proposed in the past decades for computing sliding block displacements based on various characteristics of ground shaking and the yield acceleration. These empirical displacement models are from the regression analysis of thousands of cases in which the complete sliding block analysis was conducted. Ground motion parameters (GMs), such as Peak Ground Acceleration (PGA), Peak Ground Velocity (PGV), mean period of ground motion (T_m) and Arias Intensity (I_a), have been used individually or in combination to represent the level of ground shaking in empirical displacement models. The general form of an empirical displacement model is expressed as:

$$\ln(D) = f(k_y, \text{GMs}) \quad \text{(Error! No text of specified style in document..3)}$$

Here, the natural logarithm of the predicted sliding displacement (D) is a function of the yield acceleration and the ground motion parameters (GMs). The most commonly available ground motion parameters for seismic hazard predictions are PGA, response spectral acceleration, and PGV. The key to estimating the displacement is an estimate of k_y for the slope and the expected ground motion parameters at the site.

Bray and Travararou (2007), Jibson (2007), and Rathje and Saygili (2009) have proposed empirical displacement models for rigid sliding masses that use PGA to represent the level of ground shaking and earthquake magnitude (M) to provide an indirect measure of frequency content. Because only one ground motion parameter is used in these models, they are considered scalar models. If more than one ground motion parameter is included in an empirical model, the standard deviation (i.e., variability) of the predicted sliding displacement can be significantly reduced (Saygili and Rathje 2008). Saygili and Rathje (2008) proposed a rigid sliding block model using PGA and PGV as the ground motion parameters, and such a model is a vector model

2.2 Input Parameters

To produce a seismic landslide hazard map, displacements must be predicted across a regional area containing hundreds of thousands to millions of sites. The input parameters for the analysis (e.g., slope angle, shear strength) take on different values at different locations. In a Geographic Information System (GIS), such location-dependent data is stored as raster data (Figure 2.3), which is made of small square grid cells (typical cell sizes are the scale of meters). An entire study area can be divided into millions of grid cells, each storing a single value. The resolution of a raster data describes the detail level of the data. Finer resolution means smaller grid cells, more detail and larger storage space.

The spatial distribution of the yield acceleration k_y , which represents the sliding resistance of a slope, is the critical slope parameter for predicting sliding displacement and needs to be computed for each grid cell in the study area. As noted above, the most common type of earthquake-induced landslide is a thin, veneer slope failure, so the infinite slope model can be used to calculate k_y (Equations 2.1 and 2.2). This approach allows the k_y of each grid cell to be computed easily. Each grid cell is treated as an independent infinite slope, which may not be

realistic for all types of landslides but it is the most practical way to perform a regional analysis. Slope stability analysis of finite slopes using circular or non-circular failure surfaces would be too difficult to be applied for seismic landslide hazard mapping, because 1) it requires much more site information (e.g. soil profiles), 2) the geometry of slopes are different from one location to another, and 3) the number of slopes is incredibly large in a region. However, slope stability analysis of detailed geometries of finite slopes can be used in site-specific analysis of the slopes that are identified by the seismic landslide hazard mapping.

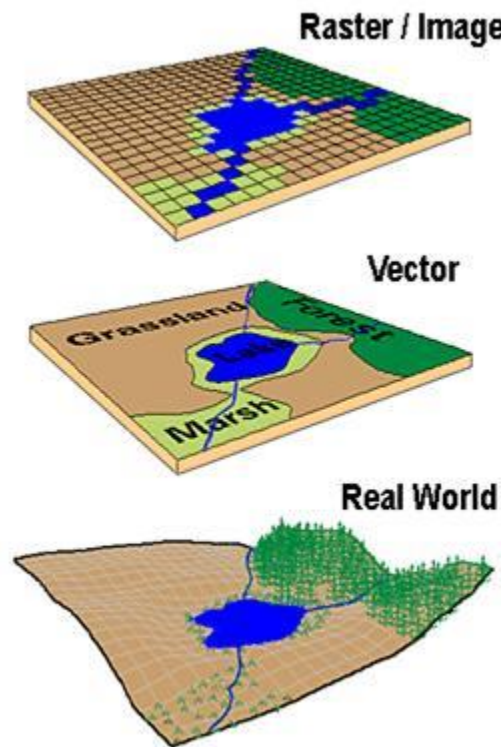


Figure 2.3 Raster and vector data for a region (http://www.sfu.ca/rdl/GIS/tour/gis_wrk.html)

The infinite slope model requires slope angle, shear strength and ground water condition for the computation of k_y . Each of these input parameters are stored in raster format so that k_y can be computed for each grid cell. The calculation of the input parameters within the GIS is described below. A region within Niigata Prefecture, Japan is used to demonstrate the process.

A Digital Elevation Model (DEM), which contains the elevation at the center of each grid cell (e.g. Figure 2.4), is used to compute the slope angle of each grid cell. The slope angle is computed for a center grid cell by using its elevation data and its eight adjacent grid cells. A slope map (e.g. Figure 5) can be created using this slope algorithm as incorporated within the Slope tool in the ArcGIS© software developed by the Environmental Systems Research Institute (ESRI).

The shear strength data required for the k_y calculation are usually derived from a geologic map. A geologic map (Figure a) is made of polygons, and each polygon represents a single geologic unit. Polygons are vector data in the GIS framework (Figure 2.3), and they need to be converted into raster data for further computation. The conversion divides polygons into raster grid cells, and each grid cell obtains a single value from the polygon to which it belongs. Shear strengths are assigned to each geologic unit prior to the conversion. Because there are two shear

strength parameters (c and ϕ), a separate cohesion map and friction angle map are developed from the geologic map (Figure 2.6b and c).

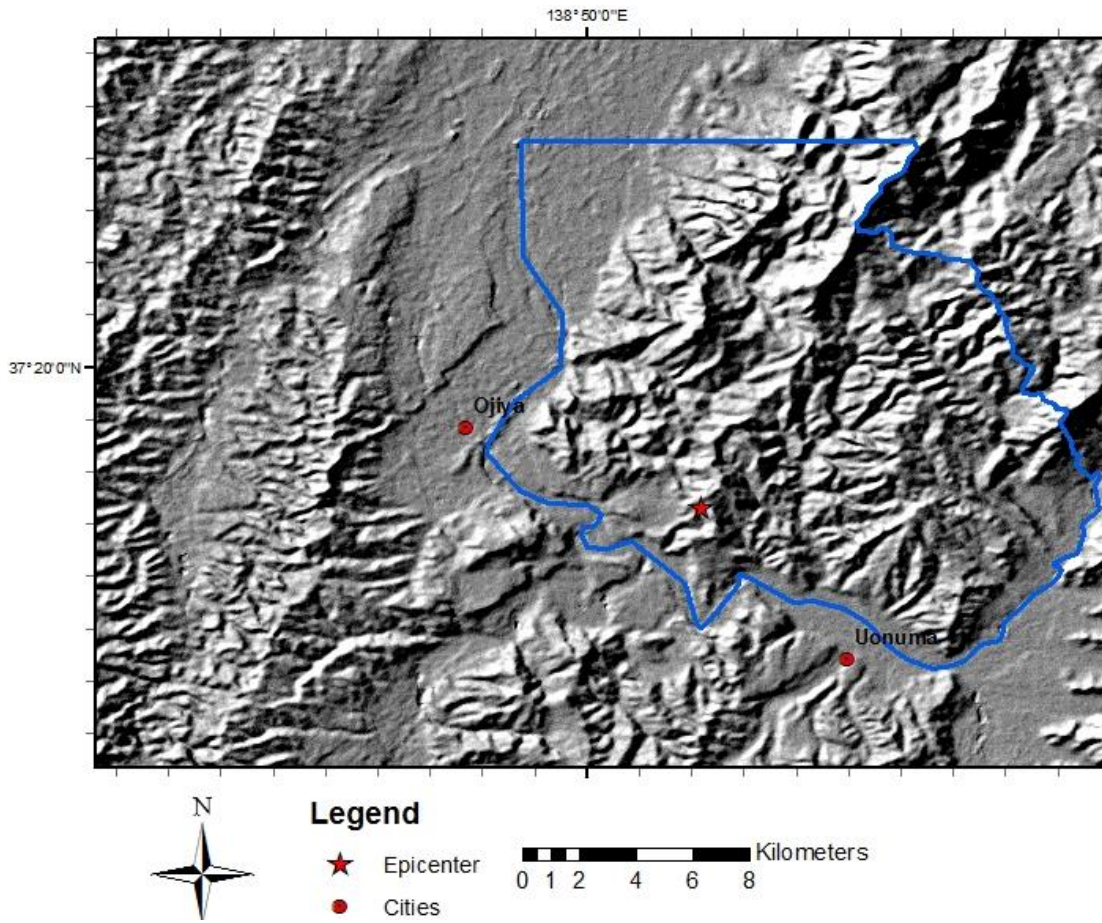


Figure 2.4 Hillshade DEM in Niigata Prefecture, Japan

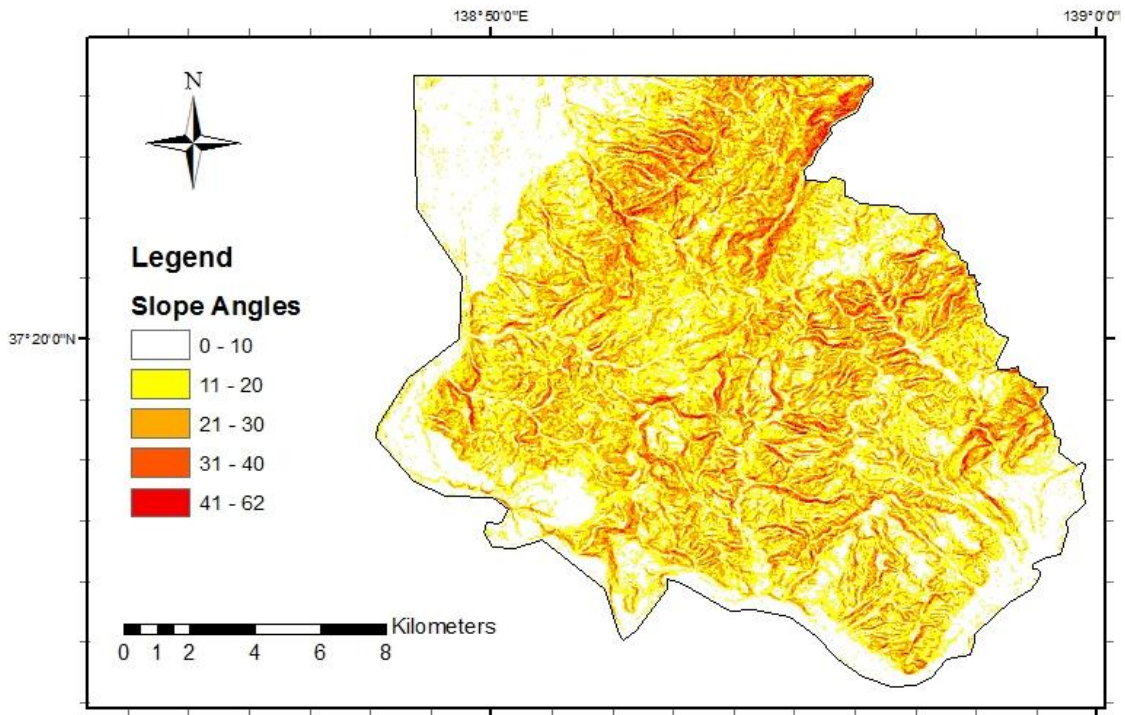
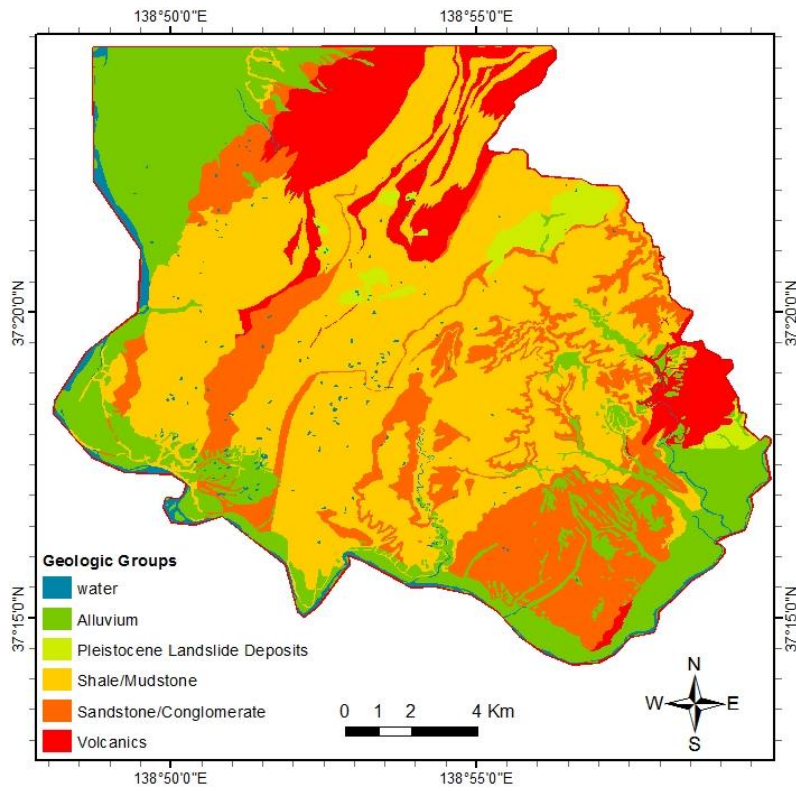


Figure 2.5 Slope map in Niigata Prefecture, Japan



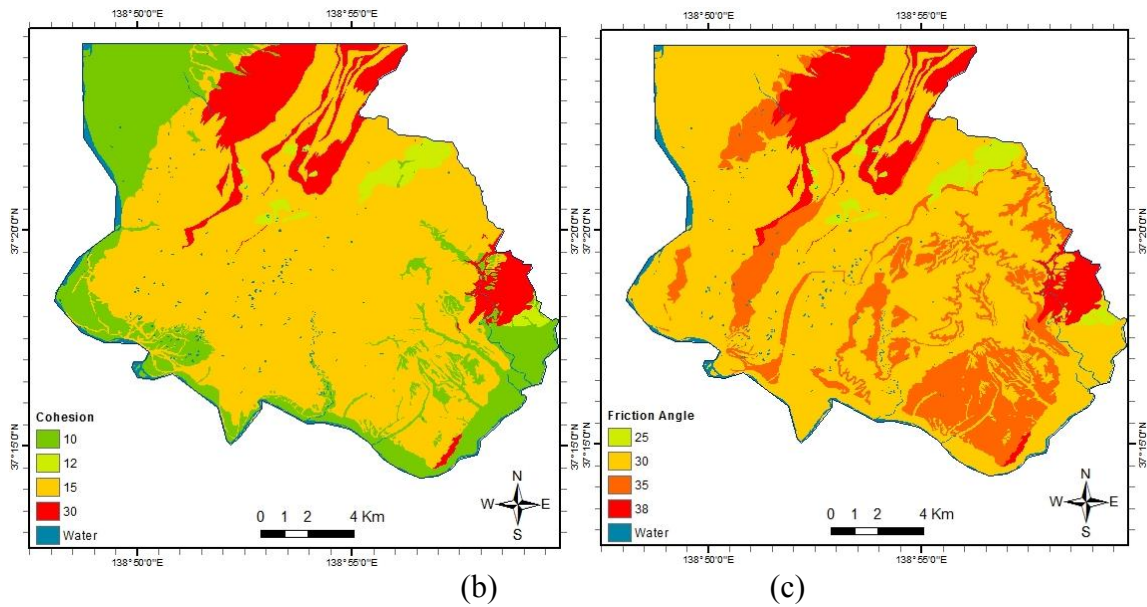


Figure 2.6 (a) Geologic map, (b) cohesion map, and (c) friction angle map for Niigata Prefecture, Japan

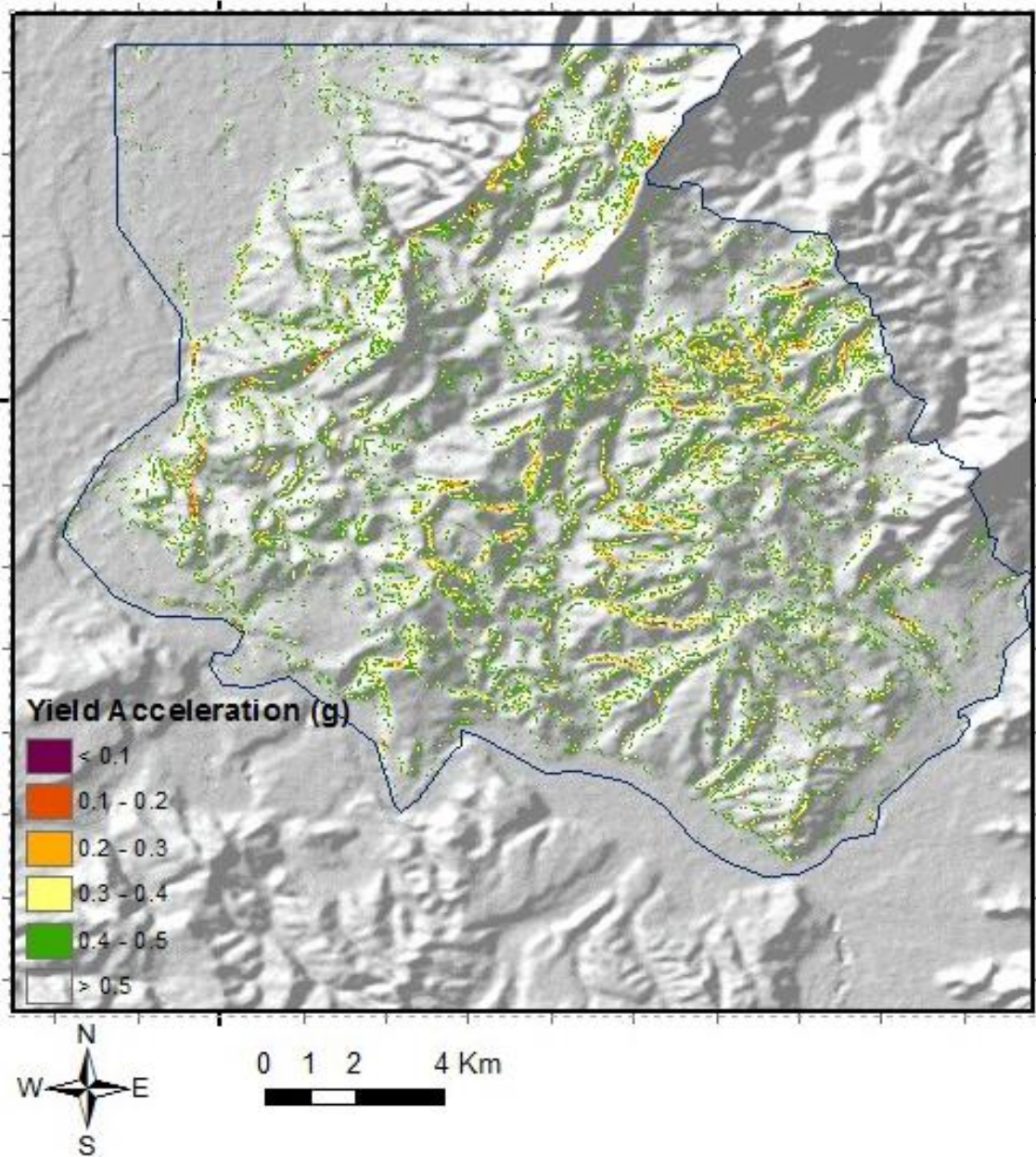


Figure 2.7 Yield acceleration map of Niigata, Japan

The other inputs for the calculation of k_y are t (slope normal thickness), m (proportion of block thickness that is saturated), and γ (unit weight of soil). These values commonly are assigned as constant values across the study area in the deterministic approach. The t value, which represents the failure depth of shallow landslides, is typically up to several meters (e.g., Kieffer et al. 2006, Keefer 2002, Jibson et al. 2000, Parise and Jibson 2000, Harp and Jibson 1996). The value of t can be determined from the thickness of surficial weak soils underlain by stiff soil or rock layer, or from observations of local shallow failures. The m value, which represents the pore water pressure on the failure surface, depends on the ground water table and may fluctuate due to seasonal change and precipitation. In deterministic analysis, the selected m value often is selected to represent the most unfavorable conditions for seismic landslides, so that

seismic landslide hazard map is conservative. The unit weight of soil γ can be assigned differently to each geologic unit if there are available testing results. However the difference in γ values is usually small, so that using a constant γ value across the study area is convenient for the k_y computation. Jibson et al. (2000) used $t = 2.4$ m, $m = 0$ and $\gamma = 15.7$ kN/m³ for the Oak Mountain quadrangle in southern California, because such values are representative for local conditions. With all above-mentioned input data, a yield acceleration map (e.g. Figure) is created by applying Equations 2.1 and 2.2 to each grid cell. Combined with ground motion parameters, the sliding displacement in each grid cell is predicted by empirical models.

For ground motion parameters, it is not practical to obtain a ground motion hazard curve for each grid cell due to the heavy computation required; additionally there will be almost no difference in the hazard curves for adjacent cells and little difference within a study area (typically smaller than 25 km by 25 km). The seismic hazard curves provided by USGS are based on the NSHM 2008 Gridded Data, which has 0.05 degree increments in longitude and latitude. It means that the seismic hazard curve is assumed to be the same within a distance range of several kilometers. Using the same seismic hazard across a study area may not be rigorous, but it simplifies the analysis without introducing large errors. Therefore, ground motion hazard curves are selected at a representative location within the study area and the same curves are used for the entire study area. Of course, if the area to be analyzed is too large to have a consistent seismic hazard, such area should be divided into several smaller areas and one set of ground motion hazard curves assigned to each smaller area.

2.3 Deterministic Seismic Landslide Hazard Map

A deterministic seismic landslide hazard map is created for ground shaking associated with a given seismic hazard level. To develop this type of map, a sliding displacement map is computed by applying an empirical displacement model to the yield acceleration map along with the ground shaking level. Such computation can be carried out by the Map Algebra tool in the ArcGIS© software.

The ground motion parameters required by empirical models are obtained from ground motion hazard curves at a given seismic hazard level. Only one set of ground motion hazard curves is used for the entire study area. Figure 2.8 is a PGA hazard curve that provides the seismic hazard level (i.e., annual frequency of exceedance) for different values of PGA at a location of interest. The two most commonly used hazard levels are 0.0021 1/yr (i.e., 10% probability of exceedance in 50 years) and 0.0004 1/yr (i.e., 2% probability of exceedance in 50 years). These hazard levels represent 475-year and 2475-year return periods for a motion, respectively. For the PGA hazard curve in **Error! Reference source not found.**, the 10% in 50 year motion is 0.54 g and the 2% in 50 year motion is 0.88 g.

A deterministic seismic landslide hazard map is produced by computing displacements at each grid cell using the ground motion level and k_y , and comparing the predicted sliding displacement map with the displacement thresholds that define the seismic hazard categories (Table **Error! No text of specified style in document.**1). An example of a deterministic seismic landslide hazard map is given in Figure for the Anchorage, Alaska area. This map uses ground motions with a 2% probability of exceedance in 50 years (e.g. PGA=0.69 g for Anchorage).

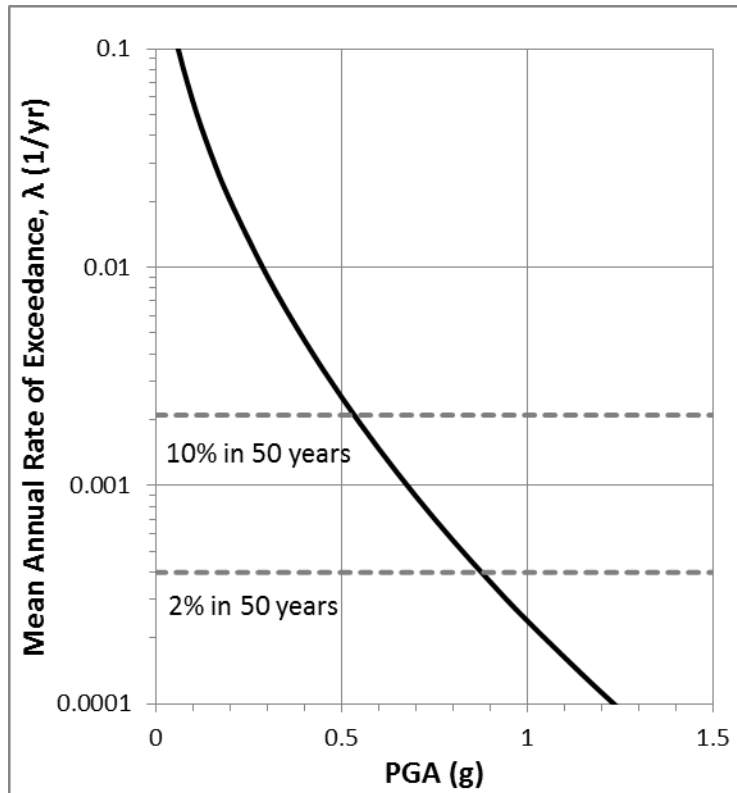


Figure 2.8 PGA Hazard Curve for a site in northern California (Rathje and Saygili 2011)

Table Error! No text of specified style in document..1 Seismic Hazard Categories based on Sliding Displacement (Jibson and Michael 2009)

Hazard Category	Sliding Displacement (cm)	Probability of Landslide (%)
Low	0 - 1	0 - 2
Moderate	1 - 5	2 - 15
High	5 - 15	15 - 32
Very High	> 15	> 32

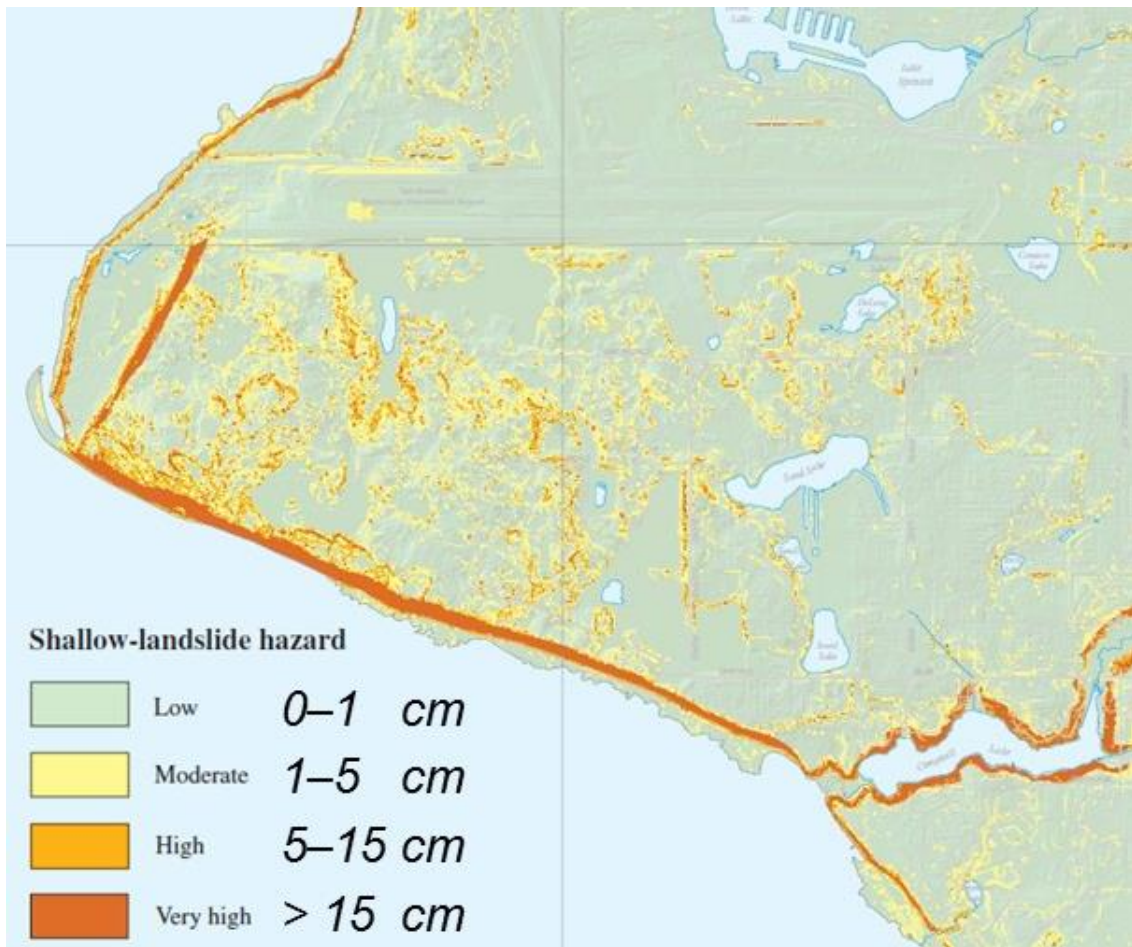


Figure 2.9 Deterministic Seismic Landslide Hazard Map for 2% probability of exceedance in 50 years in Anchorage, Alaska (Jibson and Michael 2009)

3.0 PROBABILISTIC APPROACH TO SEISMIC LANDSLIDE HAZARD MAPPING

3.1 Displacement Hazard Curves

The probabilistic approach to seismic landslide hazard mapping is based on the calculation of a sliding displacement hazard curve. A displacement hazard curve is similar to a ground motion hazard curve (e.g. **Error! Reference source not found.**), but it provides the seismic hazard level (i.e. mean annual rate of exceedance) for different levels of sliding displacement. Rathje and Saygili (2008) proposed a scalar approach, which utilizes an empirical displacement model with only one (i.e., a scalar) ground motion parameter (typically PGA), to compute a displacement hazard curve from a ground motion hazard curve. The standard deviation σ_{InD} of the empirical displacement model is included in the computation of the displacement hazard curve. Later, Saygili and Rathje (2009) modified their scalar approach by adding earthquake magnitude (M), because the scalar empirical model without magnitude did not provide unbiased estimates of the sliding displacement relative to magnitude.

In the scalar approach, the mean annual rate of exceedance (λ_D) for a displacement level x is defined as:

$$\lambda_D(x) = \sum_i \sum_k P[D > x | \text{PGA}_i, M_k] \cdot P[M_k | \text{PGA}_i] \cdot P[\text{PGA}_i] \quad (\text{Error! No text of specified style in document.4})$$

where D is sliding displacement, $P[D > x | \text{PGA}_i, M_k]$ is the probability of $D > x$ given the occurrence of acceleration level PGA_i and earthquake magnitude M_k , $P[M_k | \text{PGA}_i]$ is the conditional probability of M_k given PGA_i , and $P[\text{PGA}_i]$ is the mean annual probability of occurrence of ground motion level PGA_i . The double summation represents numerical integration over bins for PGA and M , and it represents the combined application of the total probability theorem and conditional probability.

For a given PGA_i and M_k , the empirical model provides a lognormal distribution of the displacement with mean μ_{InD} (or median $D = \exp(\mu_{\text{InD}})$) and standard deviation σ_{InD} . Given a displacement level x , the probability of $D > x$ can be calculated by using the cumulative distribution function for the normal distribution as:

$$P[D > x | \text{PGA}_i, M_k] = 1 - \Phi\left(\frac{x - \mu_{\text{InD}}}{\sigma_{\text{InD}}}\right) \quad (\text{Error! No text of specified style in document.5})$$

$P[\text{PGA}_i]$ is the annual probability of occurrence of acceleration level PGA_i and it can be approximated from the annual probability of exceedance as:

$$\begin{aligned}
P[\text{PGA}_i] &= P\left[\text{PGA} > \text{PGA}_{i-\frac{1}{2}}\right] - P\left[\text{PGA} > \text{PGA}_{i+\frac{1}{2}}\right] \\
&= \frac{P[\text{PGA} > \text{PGA}_{i-1}] + P[\text{PGA} > \text{PGA}_i]}{2} \\
&\quad - \frac{P[\text{PGA} > \text{PGA}_i] + P[\text{PGA} > \text{PGA}_{i+1}]}{2} \\
&= \frac{\lambda_{i-1} + \lambda_i}{2} - \frac{\lambda_i + \lambda_{i+1}}{2} = \frac{\lambda_{i-1} - \lambda_{i+1}}{2}
\end{aligned}$$

(Error! No text of specified style in document..6)

where $P[\text{PGA} > \text{PGA}_{i-1/2}]$ and $P[\text{PGA} > \text{PGA}_{i+1/2}]$ represent the annual probability of exceedance associated with PGA values halfway between adjacent PGA values (i.e. PGA_{i-1} , PGA_i and PGA_{i+1}). Assuming that the annual probability and annual rate of exceedance are approximately the same for rare events, the hazard values λ_{i-1} , λ_i and λ_{i+1} from the PGA hazard curve can represent the annual probability of exceedance of PGA_{i-1} , PGA_i and PGA_{i+1} .

$P[M_k|\text{PGA}_i]$ can be derived from the seismic hazard deaggregation for PGA, which is available on the USGS website or is commonly provided with a site-specific PSHA. The seismic hazard deaggregation describes the contributions of all combinations of earthquake magnitude (M_k) and source-to-site distance (R_i) given a PGA level. The sum of all contributions to a given PGA hazard level is equal to 1.0. The expression of a hazard deaggregation is $P[M_k, R_i|\text{PGA} > \text{PGA}_i]$. Therefore, the conditional probability $P[M_k|\text{PGA}_i]$ can be obtained from the total probability theorem as (Bradley 2010):

$$P[M_k|\text{PGA}_i] = \sum_l P[M_k, R_l|\text{PGA}_i]$$

(Error! No text of specified style in document..4)

$$P[M_k, R_l|\text{PGA}_i] = \frac{P[M_k, R_l, \text{PGA} > \text{PGA}_{i-1/2}] - P[M_k, R_l, \text{PGA} > \text{PGA}_{i+1/2}]}{P[\text{PGA}_i]}$$

(Error! No text of specified style in document..5)

$$P[M_k, R_l, \text{PGA} > \text{PGA}_{i-1/2}] = \frac{P[M_k, R_l, \text{PGA} > \text{PGA}_{i-1}] + P[M_k, R_l, \text{PGA} > \text{PGA}_i]}{2}$$

(Error! No text of specified style in document..6)

$$P[M_k, R_l, \text{PGA} > \text{PGA}_i] = P[M_k, R_l|\text{PGA} > \text{PGA}_i] \cdot P[\text{PGA} > \text{PGA}_i]$$

(Error! No text of specified style in document..7)

The two terms in the numerator of Equation 3.5 can be computed via Equation 3.6. Equation 3.7 is used to compute the two terms on the right side of Equation 3.6.

A displacement hazard curve is created by using Equation 3.1. Figure **Error! No text of specified style in document..** shows a displacement hazard curve for a site in northern California (Figure 2.8) and deterministic displacement values from the same PGA hazard curve used for the displacement hazard curve. The scalar probabilistic approach results in larger displacements (67 cm and 208 cm) than the deterministic approach (43 cm and 113 cm) due to the consideration of aleatory variability.

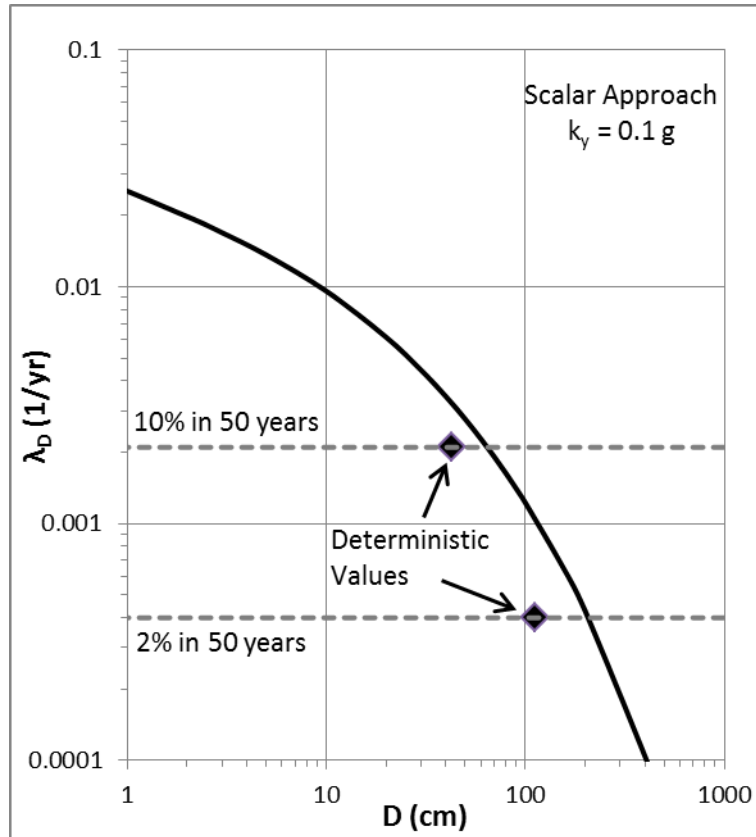


Figure Error! No text of specified style in document..1 Displacement hazard curve for a site in northern California using the scalar approach

If more than one ground motion parameter is included in an empirical model, the aleatory variability in the sliding displacement predictions can be significantly reduced (Saygili and Rathje 2008). Saygili and Rathje (2008) proposed several vector empirical displacement models (i.e., models that use a vector of ground motion parameters), and the model that includes both intensity (PGA) and frequency content (PGV) parameters was preferred to use for the vector probabilistic approach (Rathje and Saygili 2008). Similar to the scalar approach, for the vector approach the mean annual rate of exceedance (λ_D) for a displacement level x is defined as:

$$\lambda_D(x) = \sum_i \sum_j P[D > x | PGA_i, PGV_j] \cdot P[PGA_i, PGV_j] \quad \text{(Error! No text of specified style in document..8)}$$

where $P[D > x | PGA_i, PGV_j]$ is the probability of $D > x$ given ground motion levels PGA_i and PGV_j , and $P[PGA_i, PGV_j]$ is the joint annual probability of occurrence of ground motion levels PGA_i and PGV_j .

For given values of PGA_i and PGV_j , a vector predictive model provides a lognormal distribution of the sliding displacement with mean $\mu_{\ln D}$ and standard deviation $\sigma_{\ln D}$. Given a displacement level x , the probability of $D > x$ can be calculated by using Equation 3.2. $P[PGA_i, PGV_j]$ can be computed using a vector PSHA computer code (VPSHA, Bazzurro and

Cornell 2002). Alternatively, the joint probability $P[PGA_i, PGV_j]$ can be derived from the scalar hazard information for PGA along with the seismic hazard deaggregation, GMPEs for PGA and PGV, and the correlation coefficient between PGA and PGV. See Bazzurro (1998) and Rathje and Saygili (2009) for more details.

Figure **Error! No text of specified style in document.** shows hazard curves for displacement computed using the scalar and vector approaches for the same site as Figure **Error! No text of specified style in document.** As shown in Figure **Error! No text of specified style in document.**, the vector approach predicts smaller displacements than the scalar approach at all seismic hazard levels. These reductions occur because more ground motion information is utilized in the vector approach (i.e., PGA and PGV vs. only PGA), so that the vector empirical displacement model predicts a smaller median displacement and a smaller standard deviation than the scalar empirical displacement model.

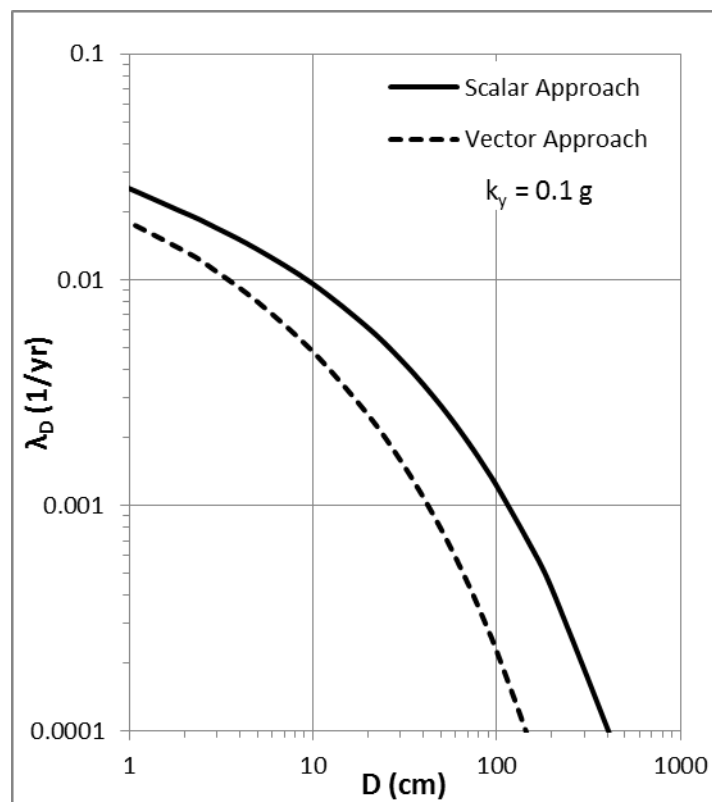


Figure **Error! No text of specified style in document.**2 Displacement hazard curves for a site in northern California using both scalar and vector approaches

The probabilistic approach incorporating aleatory variability utilizes a displacement hazard curve to define the displacement associated with a given hazard level. This approach utilizes only one representative set of ground motion hazard curves for an entire region and ignores epistemic uncertainties in the slope properties. Ignoring epistemic uncertainties allows the probabilistic approach to be applied through the use of yield acceleration thresholds that correspond with the displacement thresholds associated with each seismic landslide hazard category.

In the deterministic approach, the k_y value that produces each of the displacement thresholds associated with a seismic landslide hazard category (Table 2.1) is determined from the empirical

displacement model and the deterministic ground motion. These k_y values are defined as k_y thresholds, and they are equivalent to the displacement thresholds. These k_y thresholds are used with a yield acceleration map, in which k_y is computed for each grid cell, to identify the seismic landslide hazard category for each grid cell. This approach provides the same result as computing the deterministic displacement for each grid cell and applying the displacement thresholds.

When epistemic uncertainty is not taken into account, the k_y -threshold approach can also be applied to the probabilistic framework (Saygili and Rathje 2009). In the probabilistic case, displacement hazard curves are computed for a range of k_y values using the representative ground motions hazard curves for the study area. The displacement hazard curves are used to identify the k_y values that produce a given displacement threshold (e.g. 15 cm) for a specified seismic hazard level (e.g. 10% probability of exceedance in 50 years). These k_y values are defined as the k_y thresholds. For example, Figure shows displacement hazard curves for three k_y values (0.21 g, 0.16 g and 0.12 g), which exactly produce the displacement thresholds of 5 cm, 15 cm and 30 cm associated with a 10% probability of exceedance in 50 years. These k_y thresholds are applied to the yield acceleration map to create a probabilistic seismic landslide hazard map. For example, grid cells with k_y between 0.16 g and 0.21 g will have predicted sliding displacements between 5 cm and 15 cm, and they assigned a high seismic landslide hazard. Since only hazard categories, not the exact predictions of sliding displacements, are shown on a seismic landslide hazard map, the k_y -threshold approach is equivalent to the displacement-threshold approach.

The k_y -threshold approach avoids the computation of displacement hazard curves for each grid cell, thus it saves huge computational efforts in the probabilistic seismic landslide hazard mapping. However, the epistemic uncertainties in slope properties cannot be taken into account in this approach.

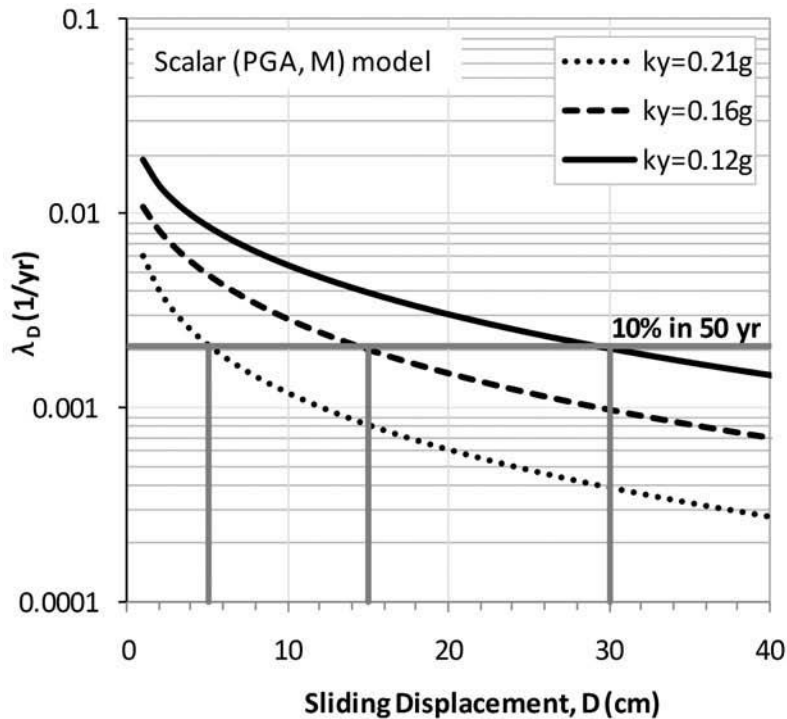


Figure 3.3 Displacement hazard curves for determining k_y thresholds (Saygili and Rathje 2009)

3.2 Logic-Tree Approach

Uncertainties always exist when characterizing the slope properties (e.g., soil shear strengths, ground water conditions, and sliding block thickness) for stability analysis. Ignoring these epistemic uncertainties and assuming a single set of slope properties leads to a single value of k_y , which simplifies the computation of the sliding response of the slope, but it may lead to an inaccurate assessment of the seismic slope performance during earthquakes.

3.2.1 Background

A logic tree analysis can be used to account for epistemic uncertainties in the assessment of the seismic slope stability hazard (Saygili 2008). A logic tree is made of nodes and branches, as illustrated in Figure Error! No text of specified style in document... Nodes represent the input parameters under consideration and the branches associated with a node represent discrete, possible values for that parameter. Each branch is associated with a weight, and the weights from all branches from one node must equal 1.0. Following branches through each node defines the input parameters for a single k_y value and the product of the weights of the branches represents the weight associated with that k_y .

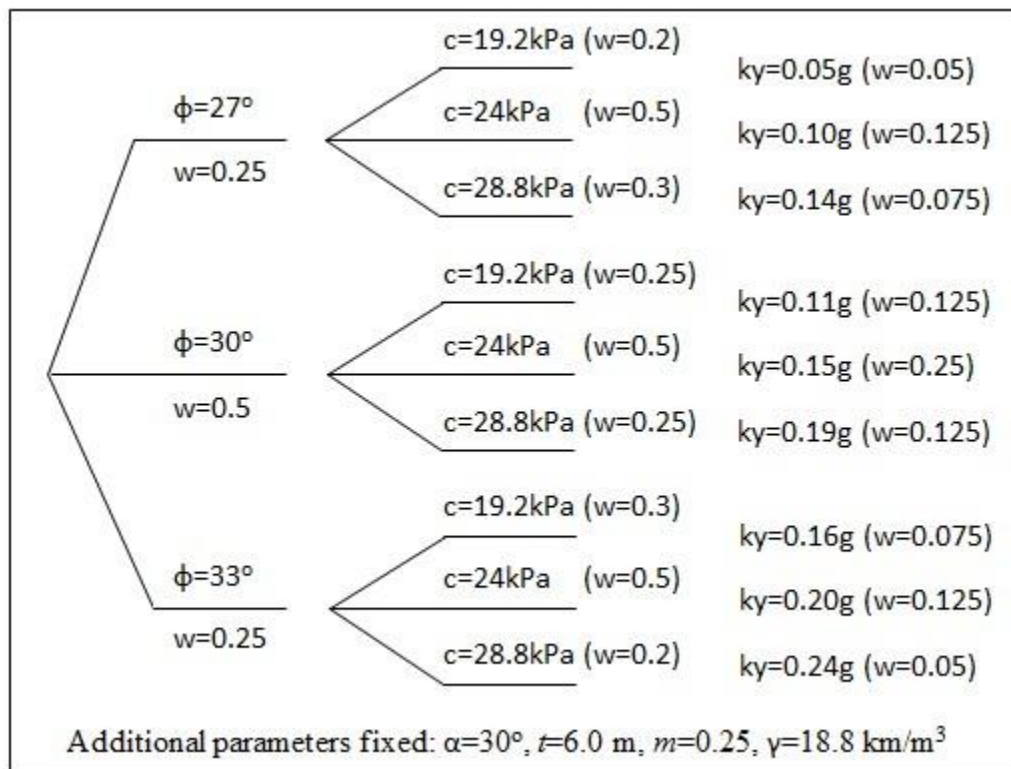


Figure Error! No text of specified style in document...4 Example logic tree for the assessment of yield acceleration

For the logic tree shown in Figure Error! No text of specified style in document., three discrete values are assumed for both c and ϕ resulting in nine possible values of k_y computed for an infinite slope analysis. The other parameters in the infinite slope analysis (i.e., slope angle, thickness, saturation ratio, and unit weight) are held constant. To incorporate the multiple values of k_y into the seismic displacement analysis, a displacement hazard curve is computed for each k_y given the ground motion hazard curve and these curves are averaged to generate a mean hazard curve. Considering a logic tree with n values of k_y , the mean hazard for displacement x can be computed as:

$$\overline{\lambda_D}(x) = \sum_{i=1}^n w_i \cdot \lambda_D(x)_i \quad (3.9)$$

where $\overline{\lambda_D}(x)$ is the weighted mean annual rate of exceedance for displacement x , $\lambda_D(x)_i$ is the displacement hazard from the i^{th} branch of the logic tree for displacement x , and w_i is the weight associated the i^{th} branch of the logic tree.

Figure 3.5 demonstrates the calculation of the mean displacement hazard curve for the logic tree in Figure 3.4. The displacement hazard curves for the nine k_y values in the logic tree are shown by the gray curves in Figure Error! No text of specified style in document.. and the mean displacement hazard curve is shown by the solid black line. The displacement hazard curve for the best estimate $k_y = 0.15$ g ($c = 24$ kPa, $\phi = 30^\circ$ in Figure 3.4) is also shown in Figure Error! No text of specified style in document.. The mean displacement hazard curve from the logic tree analysis is higher than the hazard curve using the best estimate k_y , indicating that incorporating the epistemic uncertainty in the soil properties increases the displacement hazard. Less uncertainty in the soil properties would result in the mean hazard curve becoming more similar to the hazard curve for $k_y = 0.15$ g.

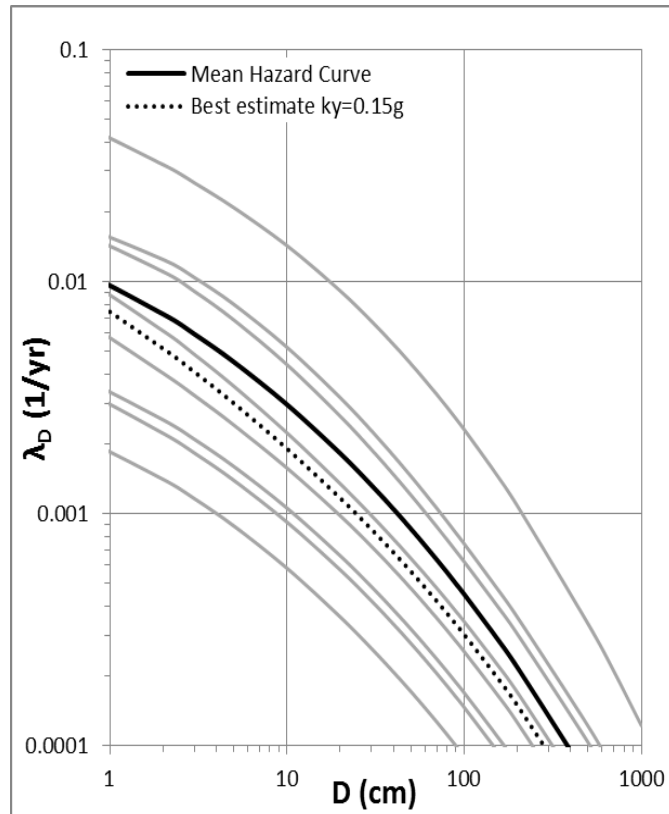


Figure Error! No text of specified style in document..5 Rigid Displacement Hazard Curves for Logic Tree

3.2.2 Development of a Logic Tree

The epistemic uncertainties in the shear strengths, m value and t value should be considered in the logic-tree analysis, because such parameters are used to determine the k_y value of each grid cell. Additionally, the epistemic uncertainty among empirical displacement models should also be considered in the logic-tree analysis.

The uncertainty in shear strengths can be estimated from lab and field testing results. However, at a regional scale the most practical way to assign uncertainty may be through published uncertainty estimates or, if available, through the variability in in situ test parameters, such as SPT blow count, across a geologic unit. As an example of published uncertainty estimates, Phoon and Kulhawy (1999) summarized that the coefficient of variance is about 10 to 50% for undrained shear strength and 5 to 15% for effective friction angle. If enough testing results are not available to evaluate the uncertainty in shear strengths, one may refer to the above coefficients of variance and use engineering judgment to develop specific values to be used in the logic-tree analysis. The weights of branches can be determined based on three-point estimation of a normal distribution.

The thickness of sliding block t is typically several meters for shallow failures. It depends on the thickness of surficial weak soil, and it is also correlated with the shear strengths of underlying soil layers. If the underlying soil layers are strong enough, the failure will be restrained in the surficial weak layer. Smaller shear strengths of underlying layers may lead to deeper landslides. Slope stability analysis may be necessary to determine the critical failure depth for complicated slope geometries. Nevertheless, the shallow-failure assumption is

generally valid and convenient for regional mapping. The selection of representative t values should be based on the knowledge of local geology and engineering observations. In the logic tree, three branches can be used to represent a typical range of t values, and a uniform distribution should be used to assign weights unless there is specific information indicating that some depths are more likely than others.

The m value, defined as the proportion of the block thickness that is saturated, is calculated by the ground water table and the t value. The ground water table will fluctuate due to seasonal changes and precipitation. Topography, seepage, and artesian water can cause complicated spatial variations of the ground water table in a region. The estimation of the ground water table relies on survey records and precipitation forecasts. Because of these complications, a uniform distribution is most likely applied to the ground water table levels. The selected ground water table levels, and corresponding m values, should represent the likely range of values indicated by observations. If one wants to incorporate the most unfavorable location of the ground water table, it can be included in the logic tree with a corresponding weight that indicates its likelihood of occurrence.

The unit weight of soil γ generally has a small variation in the same soil and a small difference between different soils. The coefficient of variance in γ is less than 10% according to Phoon and Kulhawy's study (1999). Therefore, using a constant γ value across the study area is acceptable.

Several empirical displacement models should be adopted, rather than only one model, to incorporate the epistemic uncertainty among the different models. All empirical models should be equally weighted unless some models are believed to be more accurate than others. For instance, a vector model (e.g. SR08) may be assigned a higher weight than scalar models because the vector model takes more ground motion information in the calculation and, theoretically, should provide a more accurate prediction of displacement.

Figure 3.6 shows an example logic-tree with the logic-tree components associated with shear strength, sliding block properties, and empirical models separated.

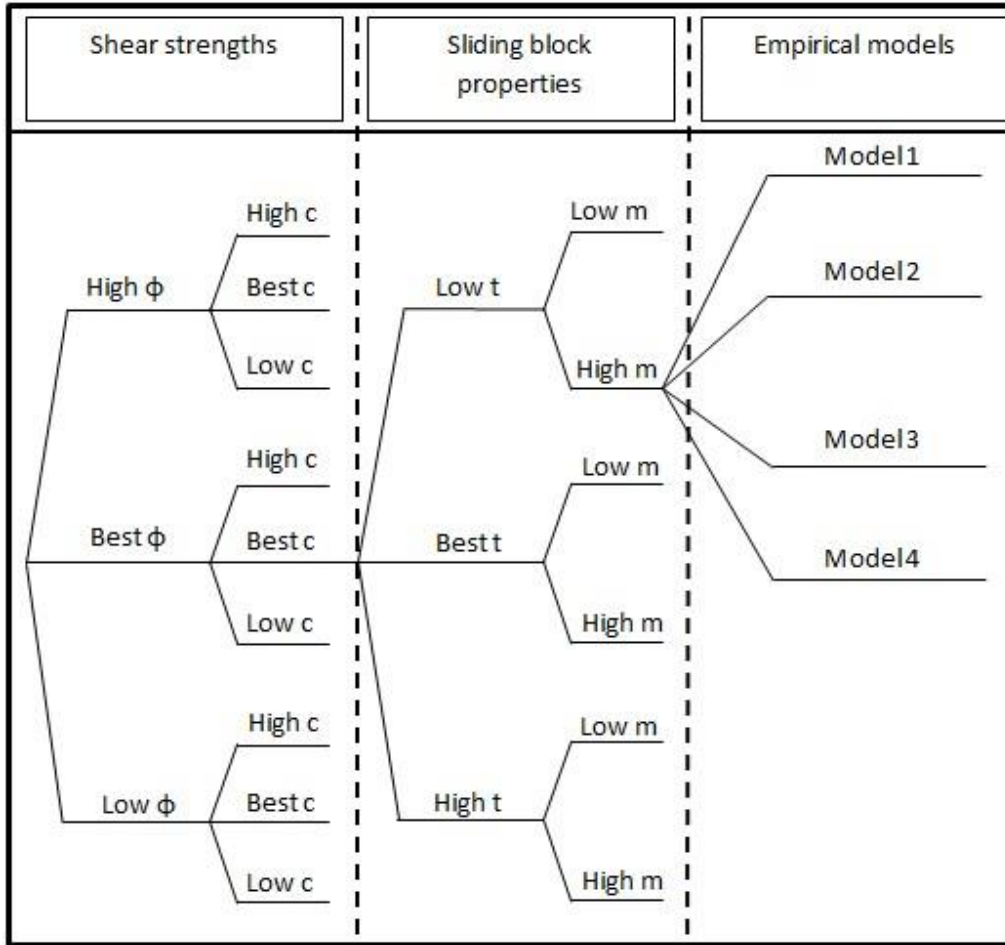


Figure 3.6 Example logic tree for probabilistic seismic landslide hazard mapping

3.2.3 Applying Logic-Tree Analysis to Seismic Landslide Hazard Mapping

When logic-tree analysis is applied to seismic landslide hazard mapping, each grid cell has dozens of possible k_y values with associated weights. Therefore, the approach of using k_y thresholds to define seismic landslide hazard categories is no longer applicable. A mean displacement hazard curve could be computed for each grid cell across an entire region but this would require a large amount of computation and is not practical. To address this issue, an efficient computational scheme is developed which does not sacrifice any accuracy.

The approach to applying the logic tree to regional analysis is based on computing the weighted mean annual rate of exceedance $\bar{\lambda}_D(x)$ at each grid cell for the displacement thresholds associated with the seismic landslide hazard categories. This approach is called the Mean λ_D Threshold approach. Comparing $\bar{\lambda}_D(x)$ of each grid cell and displacement threshold with the hazard level under consideration (target hazard level λ^*) allows each grid cell to be assigned to an appropriate seismic landslide hazard category. The Mean λ_D Threshold approach is illustrated using the mean displacement hazard curve shown in Figure . At $\lambda^* = 0.0021$ 1/yr, the mean displacement hazard curve indicates a sliding displacement is 8 cm for the grid cell, and this grid cell should be categorized as high seismic landslide hazard ($5 \text{ cm} < D < 15 \text{ cm}$). Alternatively, comparing λ^* with $\bar{\lambda}_D(5\text{cm})$ and $\bar{\lambda}_D(15\text{cm})$ can also provide the same result. If $\bar{\lambda}_D(5\text{cm})$ for a

grid cell is greater than $\lambda^* = 0.0021$ 1/yr, then the sliding displacement for that grid cell associated with $\lambda^* = 0.0021$ 1/yr is greater than 5 cm. If $\bar{\lambda}_D(15\text{cm})$ is less than $\lambda^* = 0.0021$ 1/yr for the same cell, then the sliding displacement for that cell associated with $\lambda^* = 0.0021$ 1/yr is smaller than 15 cm. Therefore, this grid cell is placed in the 5 to 15 cm bin, which corresponds with the high seismic landslide hazard category. Similar to the k_y -threshold approach, only hazard categories, not exact predictions of sliding displacements, are assigned to grid cells to create a seismic landslide hazard map. The Mean λ_D Threshold approach is equivalent to the displacement-threshold approach.

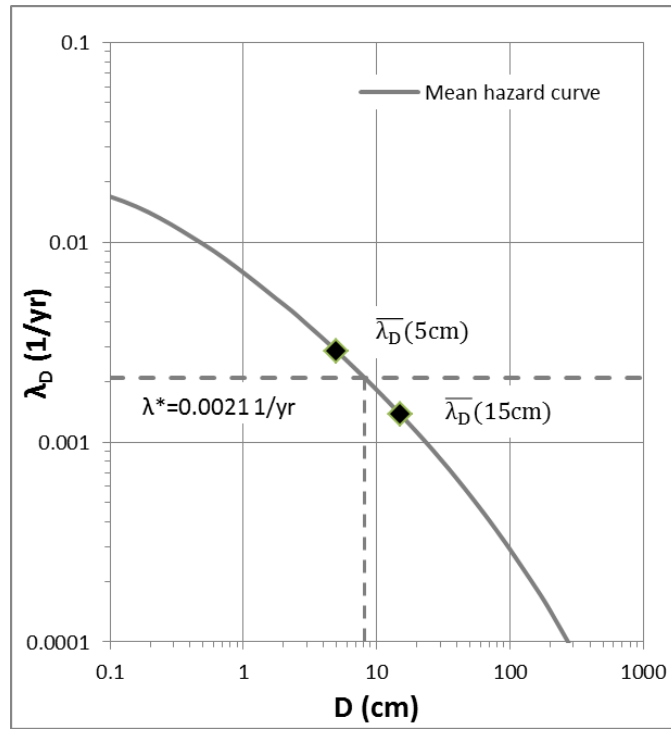


Figure 3.7 Illustration of Mean λ_D Threshold approach

The key to applying the Mean λ_D Threshold approach to each cell is the efficient computation of $\bar{\lambda}_D(x)$ from Equation 5.1 for each displacement threshold so that it can be compared with λ^* . Equation 3.9 requires the $\lambda_D(x)$ values associated with each k_y value. An interpolation relationship between k_y and $\lambda_D(x)$ is used to efficiently compute the $\lambda_D(x)$ values for Equation 3.9. The development of this interpolation relationship is described below.

For a single empirical displacement model (e.g. Rathje and Saygili 2009) and a single ground motion hazard curve, one k_y value leads to one displacement hazard curve. At a displacement threshold of x cm (e.g. $x = 5$ cm), one k_y value corresponds to one $\lambda_D(x)$ value. This concept is demonstrated in Figure for $x = 5$ cm. To establish a relationship between k_y and $\lambda_D(5\text{cm})$ for this case, $\lambda_D(5\text{cm})$ is compiled for a range of k_y values from the associated displacement hazard curves, and the data are fit with a 4th order polynomial regression model in log-log space (Figure). This relationship can then be used to quickly calculate $\lambda_D(5\text{cm})$ for a given k_y value.

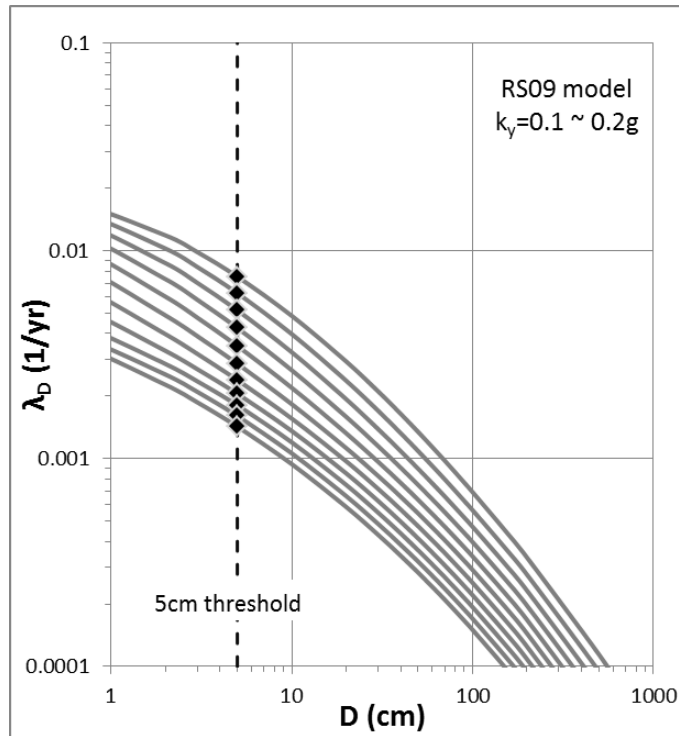


Figure 3.8 Displacement hazard curves for k_y values between 0.1 and 0.2 g

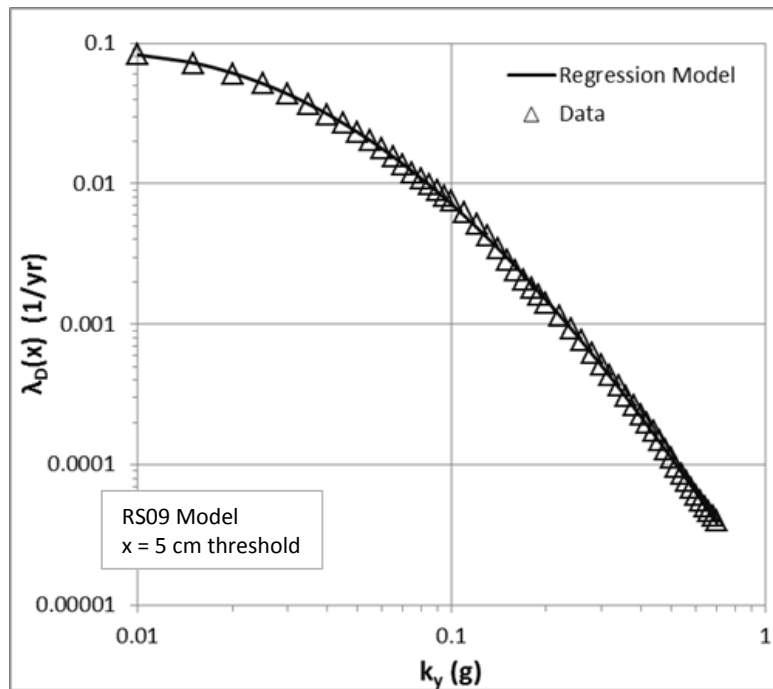


Figure 3.9 $\lambda_D(x)$ vs. k_y for $x=5$ cm and 54 k_y values between 0.01 and 0.7 g.

The typical range of k_y values of slopes that are potentially unstable during earthquakes is from 0.01 to 0.70 g. Any slope with k_y below 0.01 g is essentially statically unstable ($FS \leq 1.0$) and slopes with k_y larger than 0.70 g are either very flat or are made of strong soils/rocks, meaning that such slopes can be assumed as seismically stable. Using small k_y increments (e.g.

0.01 g) and assuming all k_y values are between 0.01 to 0.70 g, there are only several dozens of possible k_y values to consider within a study area, despite the presence of millions of grid cells. Additionally, the difference between two displacement hazard curves is very small for a small change in k_y . Figure shows a series of displacement hazard curves for k_y values between 0.1 and 0.2 g using an increment of 0.01 g, and these curves change gradually. Therefore several dozens of displacement hazard curves and interpolation between these hazard curves can be used to approximate all possible displacement curves in a region.

Relationships between $\lambda_D(x)$ and k_y can be derived for each empirical displacement model and each displacement threshold given the ground motion hazard curve for a region. The general form of the regression relationships is expressed as:

$$\ln(\lambda_D(x)) = a_1(\ln(k_y))^4 + a_2(\ln(k_y))^3 + a_3(\ln(k_y))^2 + a_4\ln(k_y) + a_5 \quad (3.10)$$

where a_1 to a_5 are coefficients of the regression model. Using the regression relationships, the multiple k_y values associated with each grid cell can be quickly related to the associated $\lambda_D(x)$ values needed for Equation 3.9 and the $\bar{\lambda}_D(x)$ of each grid cell calculated. By comparing $\bar{\lambda}_D(x)$ values for the displacement thresholds of $x = 1, 5$ and 15 cm with the target hazard level (λ^*), the seismic landslide hazard category can be determined for each grid cell.

3.2.4 Screening Analysis

To further reduce the computation time for the regional analysis incorporating epistemic uncertainties, a screening analysis using the worst-case scenario of the logic tree is carried out. The worst-case scenario is associated with the minimum k_y , and is represented by the smallest shear strength and the largest m and t values. This analysis can highlight the grid cells that have low seismic landslide potential because if the displacement hazard for 1 cm (i.e., the lower bound displacement threshold for the moderate landslide hazard category) is less than λ^* for the minimum k_y , then the displacement hazard computed using the full logic tree will also be less than λ^* . Therefore, the full logic-tree analysis does not need to be performed for these grid cells.

The screening analysis can be performed for all displacement thresholds. For larger displacement thresholds, more grid cells are excluded from the full logic-tree analysis. The screening analysis may remove as many as 70% to 90% (or even more) of the grid cells from the full logic-tree analysis.

4.0 APPLICATION OF PROBABILISTIC SEISMIC LANDSLIDE HAZARD MAPPING: ANCHORAGE, ALASKA

4.1 Study Area

To implement the approach developed for probabilistic landslide hazard mapping, Anchorage, Alaska is selected as the study area. This location was selected based on the history and occurrence frequency of earthquakes, the availability of the required data in GIS format, access to databases of soil properties in the study area, and the availability of PGV ground motion prediction models for the tectonic region.

Anchorage has experienced several large earthquakes in the past, such as the 1964 Alaska earthquake ($M_w = 9.2$). Seismic landslides caused most of the deaths and economic losses during the 1964 earthquake in Anchorage (Keefer, 1984). Since then, many studies have been conducted to identify areas susceptible to potential landslides in future earthquakes. Jibson and Michael (2009) recently created seismic landslide hazard maps for Anchorage using the deterministic approach, and thus this is an ideal study area because the data required for analysis are available.

The Anchorage, Alaska study area is about 24 km by 25 km (Area = 301 km², Figure 4.2) and represents the extent of the seismic landslide hazard map developed by Jibson and Michael (2009). The northern, western and central areas are mostly plains, and downtown Anchorage is located at the northwestern corner. The study area boundaries along the northwest to southwest are mostly coastlines. The Chugach Mountains cover the eastern and southern parts and extend beyond the boundaries of the study area.

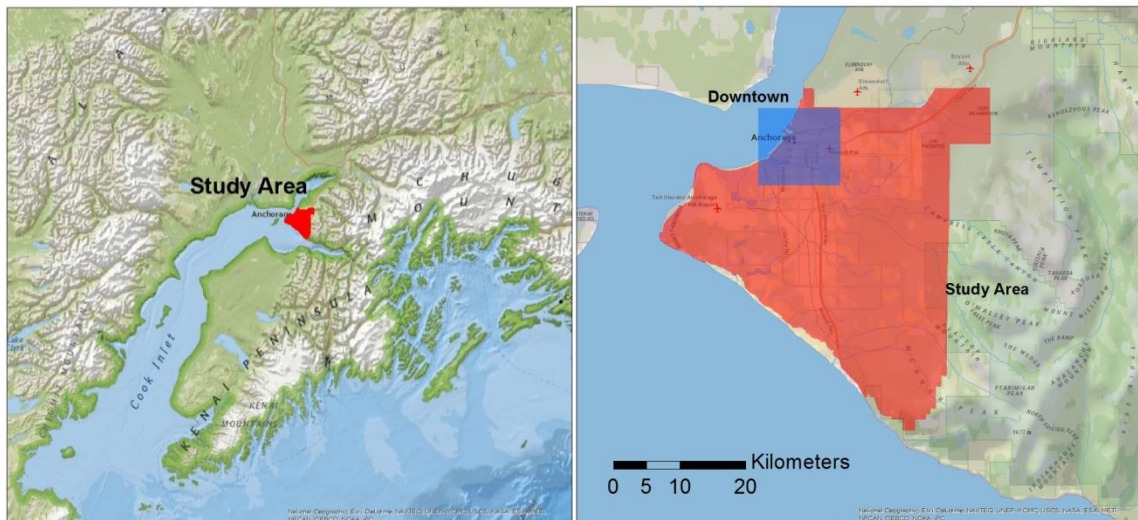


Figure 4.2 Overview of the study area in Anchorage, Alaska (based on National Geographic, ESRI)

Jibson and Michael (2009) produced seismic landslide hazard maps for Anchorage using sliding displacements predicted from a deterministic approach. The maps are based on ground motions associated with two different seismic hazard levels, 2% probability of exceedance in 50 years and 10% probability of exceedance in 50 years, which correspond to PGA values of 0.69 g and 0.43 g respectively (Wesson et al. 2007). In defining the slope properties for the calculation of the infinite slope k_y , the slab thickness (t) was assumed to be 15 m (50 ft), which is the upper

bound of commonly observed landslides in Anchorage (personal communication with Dr. Randall W. Jibson). By assuming a groundwater table at 3 m (10 ft) depth, the saturation factor (m) is relatively large at 0.8. The combination of the large slab thickness and high groundwater level is very conservative and results in small values of k_y . The unit weight of soil was held constant at 18.8 kN/m³ (120 lb/ft³) and used for the entire study area. The friction angle and cohesion intercept were assigned across the study area based on geologic units. Displacements were computed across the study area using yield acceleration values determined at 6-m (20 ft) intervals, and the empirical displacement model of Jibson (2007) that uses only PGA, without magnitude, to calculate displacement.

Figure 4.3 shows the Jibson and Michael (2009) seismic landslide hazard map given a PGA with a 2% probability of exceedance in 50 years. The landslide hazard categories are assigned from displacements using the displacement thresholds previously described in Table 2.1. For this map, about 1.5% and 2.7% of the study area are classified as high hazard (5 cm < D < 15 cm) and very high hazard (D > 15 cm), respectively. Another 5.5% of the study area was defined as moderate hazard (1 cm < D < 5 cm). Most areas with high or very high hazard are within colluvium units along the coastal bluffs and stream valleys in the lowland, colluvium units within the inland Chugach Mountains, and alluvium units along abandoned or modern stream-banks. A similar hazard map with 10% probability of exceedance in 50 years was also produced through the deterministic approach, and the results are summarized in Table 4.2. The smaller ground motions associated with this hazard level results in less of the study area assigned to the moderate, high, and very high hazard categories.

Table 4.2 Percentage of study area in each seismic landslide hazard category from deterministic map (Jibson and Michael 2009)

Hazard Category	Sliding Displacement (cm)	Percentage of Study Area	
		2% in 50 years	10% in 50 years
Low	0 - 1	90.31%	95.69%
Moderate	1 - 5	5.53%	1.63%
High	5 - 15	1.48%	0.75%
Very High	> 15	2.68%	1.93%

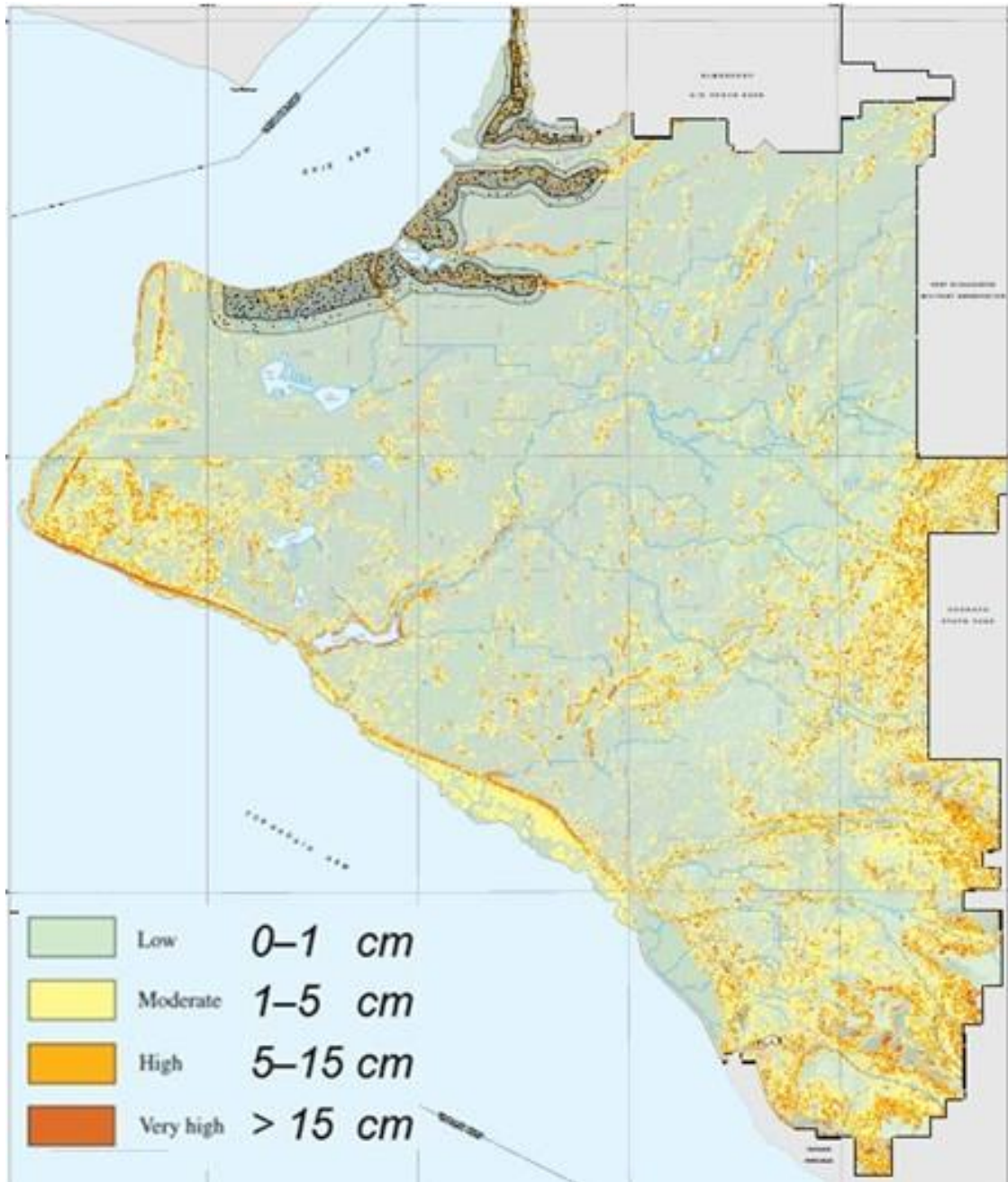


Figure 4.3 Deterministic seismic landslide hazard map at 2% probability of exceedance in 50 years of Anchorage, Alaska (Jibson and Michael 2009)

4.2 Input Data for Seismic Landslide Hazard Map

A seismic landslide hazard map requires information regarding topography, geology/shear strength, and the sliding block properties. The data used to develop this information for the study area are described below.

Figure 4.4 is a shaded relief map of the study area derived from a DEM. The entire study area is about 301 km² (8,370,622 grid cells), with a width of 24 km and a length of 25 km. The highest elevation is 1,026 m (3,363 feet) and the largest slope angle is 77°. The DEM was derived from Light Detection and Ranging (LIDAR) data produced by the Municipality of Anchorage in 2004. The original LIDAR DEM was at 1.5 m (5 ft) resolution and the vegetation and buildings had been removed. Jibson and Michael (2009) resampled the LIDAR data to a 6-m (20 ft) resolution DEM and used this DEM to generate a slope map (Figure 4.5).

The 6-m resolution DEM is used to develop the slope map (Figure 4.5) required to compute the yield acceleration information across the study area. Most of the steep terrain is along the coastal bluffs, stream valleys, and in the southern and eastern mountain areas. These locations of steep terrain are, of course, more susceptible to seismic landslides than other areas, as also seen in the deterministic seismic landslide hazard map (Figure 4.3).

Jibson and Michael (2009) used digitized versions of the surficial geologic maps of Schmoll and Dobrovolsky (1972) and Yehle et al. (1992) to assign shear strengths across the study area. There are 17 geologic units across the study area: a map of these units is shown in Figure and the shear strength properties from Jibson and Michael (2009) are listed in

Table 4.3.

The famous Bootlegger Cove Clay (bc unit) is related to the deeper landslides from the 1964 earthquake, because at depth it is weak with the potential for cyclic degradation of shear strength. However, the Bootlegger Cove Clay was assigned relatively larger shear strength when exposed at the ground surface based on the relatively larger values of SPT blowcount indicated near the surface as compared to at depth. Although the Bootlegger Cove Clay is not widely shown on the surficial geologic map, it is the main underlying soil layer of man-made fills and sand deposits.

Silt deposits (s) are along the coastal lines. The units af, al and an are alluvium on plains and along stream channels with similar shear strengths, and the glacial alluvium (ga) on irregular-shaped hills has higher shear strength. Glacial material units (gm, m and mg) all have high shear strength, and they form the underlying soil layer of most surficial geologic units in Anchorage. Sand deposits (sl and sh) cover the central west part of the study area. The colluvium unit c-bl mostly covers coastal bluffs and valley walls in the lowland. The other colluvium unit c-br is distributed in the eastern area on the slopes of the Chugach Mountains.

Sands and gravels were characterized using effective (drained) shear strengths. Clays and silts were characterized as total (undrained) shear strengths with zero friction angle. The shear strengths in

Table 4.3 are considered best estimates and were compiled by Jibson and Michael (2009) using triaxial test, direct shear, vane shear and standard penetration test (SPT) results.

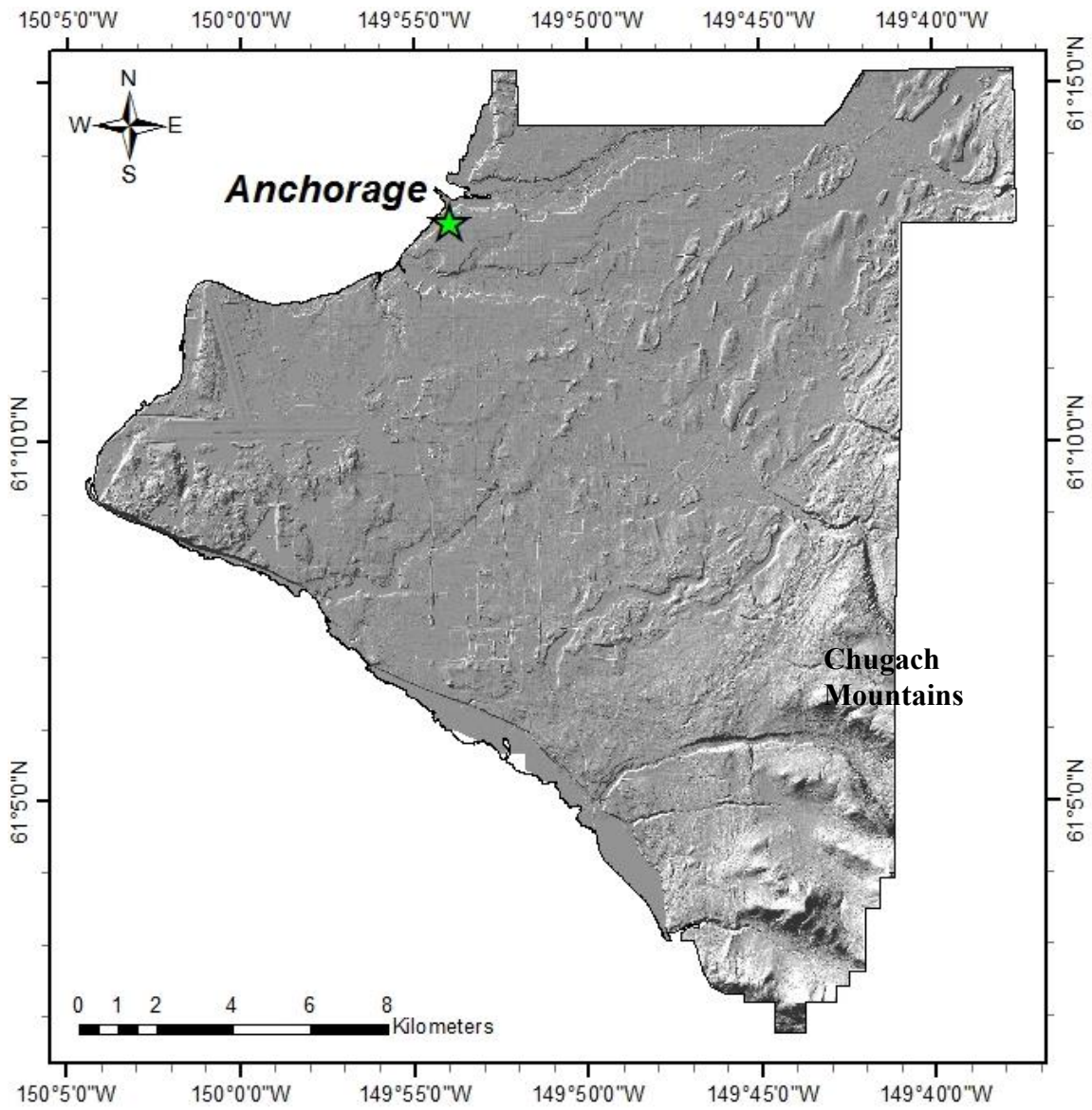


Figure 4.4 Shaded relief map of Anchorage, Alaska

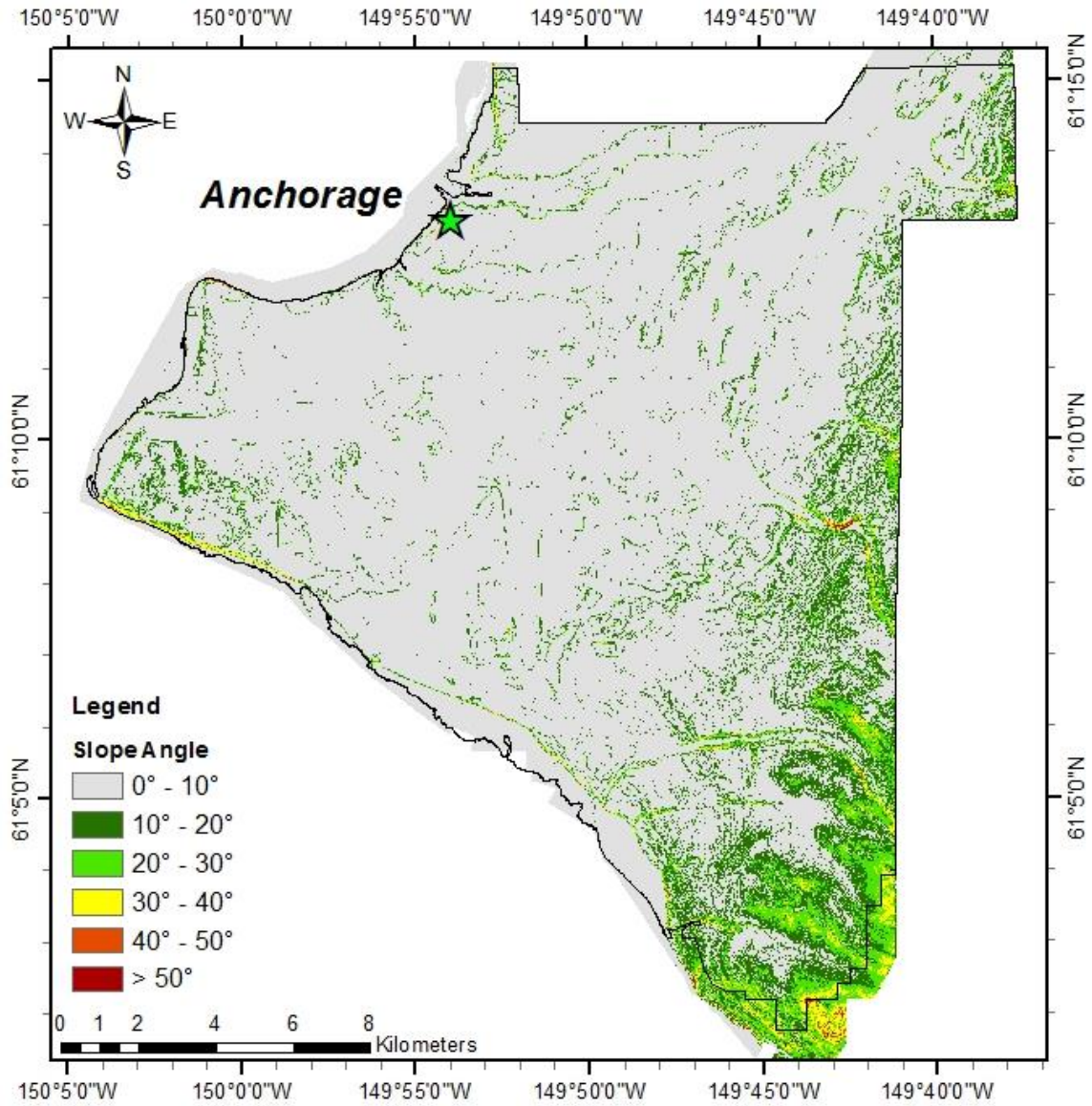


Figure 4.5 Slope map of Anchorage, Alaska

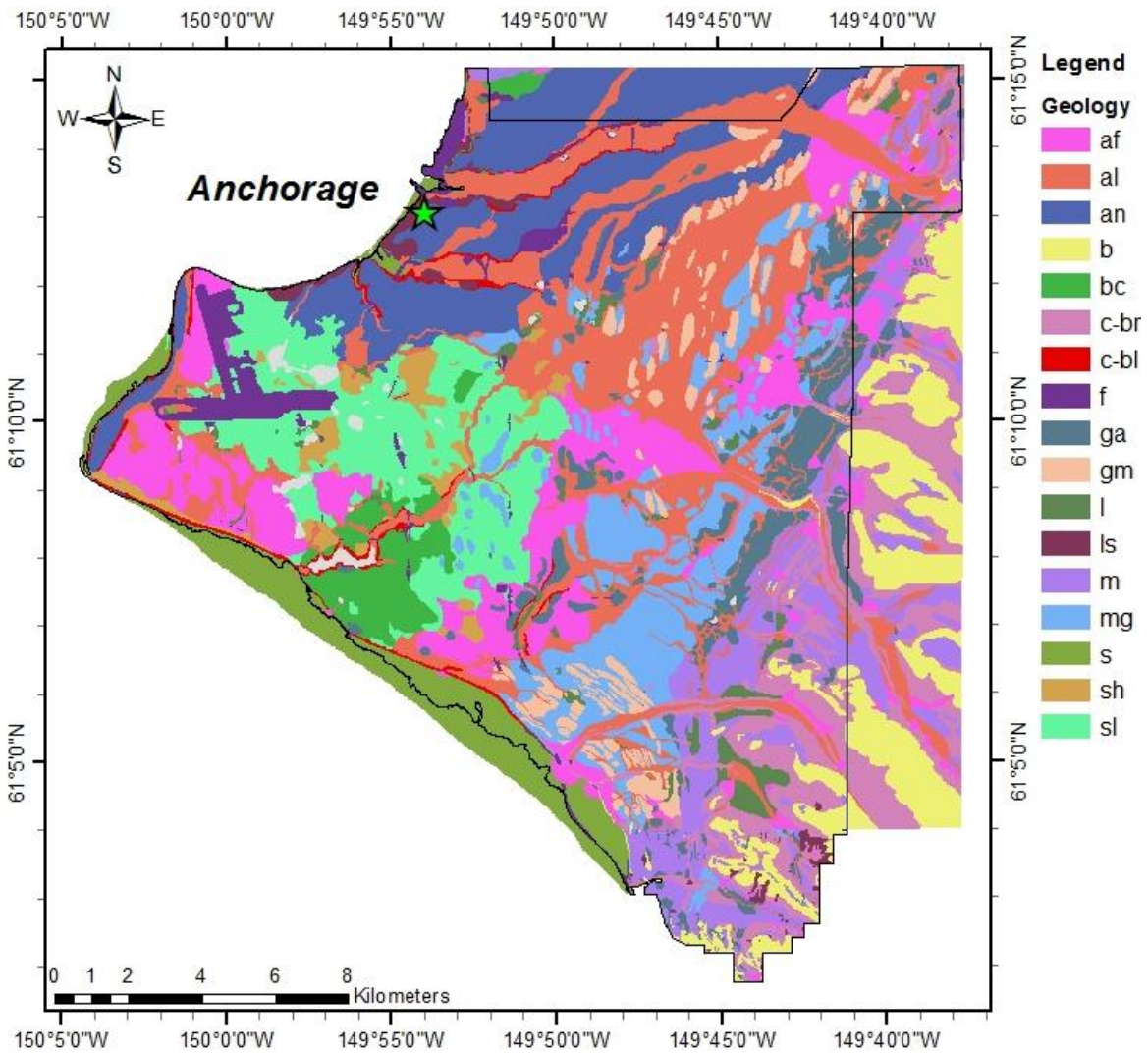


Table 4.3 Geologic Units and Shear Strengths (Jibson and Michael 2009)

units	Friction Angle (deg)	Cohesion (kPa)	Compositions
af	36	24	Deposits in alluvial fans, alluvial cones, and emerged deltas
al	36	19	Alluvium in abandoned stream channels and in terraces along modern streams
an	36	24	Coarse-grained surficial deposits
b	40	192	Bedrock
bc	0	120	Bootlegger Cove Clay
c-br	38	38	Colluvium derived from bedrock on slopes of the Chugach Mountains
c-bl	0	38	Colluvium derived from glacial materials along coastal bluffs
f	34	48	Manmade fill
ga	32	38	Glacial alluvium in irregular-shaped hills (including kames, eskers, and kame terraces)
gm	38	48	Glacial and (or) marine deposits, typically in elongate hills
l	0	144	Lake and pond deposits
ls	30	24	Landslide deposits, similar to an unit
m	38	43	Morainal deposits, generally in long ridges marking the margins of former glaciers
mg	37	38	Marine, glacial, and (or) lacustrine deposits
s	0	72	Silt
sh	34	24	Sand deposits in broad, low hills, and windblown sand deposits in cliffhead dunes near Point Campbell
sl	34	19	Sand deposits in a wide low-lying belt around Connors Lake

The variability in shear strengths can be estimated from the study of Phoon and Kulhawy (1999). They summarized that the coefficient of variation (COV, equal to the standard deviation divided by the mean) is about 10 to 50% for undrained shear strength and 5 to 15% for effective friction angle. For this study, the COV for the undrained shear strength is taken as 30%, and for the effective friction angle it is taken as 10%. The COV for the effective cohesion is taken as 20%, so that the total uncertainty in the drained shear strength is similar to the undrained shear strength. Dr. Randall W. Jibson from the USGS (personal communication) also suggested similar levels of uncertainty for shear strength based practical experience and engineering judgment in Anchorage, Alaska.

Assuming that shear strengths follow a normal distribution, the weights of the logic tree branches assigned to the high, mean and low shear strengths are determined based on a three-point estimation of the normal distribution. To approximate a standard normal distribution the three points are taken at 10%, 50%, and 90% (i.e., $\mu - 1.3\sigma$, μ , $\mu + 1.3\sigma$), the corresponding weights are 0.3, 0.4, and 0.3. The weights of the logic tree branches for shear strengths are summarized in Table 4.4.

Table 4.4 Weights of logic tree branches for shear strengths

Shear Strength	No. of σ	CDF	Weight
High	1.3	90%	0.3
Mean	0	50%	0.4
Low	-1.3	10%	0.3

The typical thickness and the underlying soil layers of the different surficial geologic units are summarized from the studies of Schmoll and Dobrovolny (1972) and Combellick (1999), as shown in Table 4.5. The underlying units are listed in order of their predominance across the main geologic unit. Such information will be used to estimate the sliding block properties (i.e., depth of failure surface) for each geologic unit.

Table 4.5 Thickness and underlying soil layers of surficial geologic units

Units	Thickness (m)	Underlying Soil Layers
al	3 ~ 9	m, gm, mg, ga, bc
an, af, ga	6 ~ 15	m, gm, mg, bc
bc	up to 18 in the sea bluffs up to 60 in the central part of lowland area	m, gm, mg
c-bl	up to 3	m, gm, mg, ga, bc
c-br	up to 3	b
f	3 ~ 6	bc, l, an, af, ga, al
l	6 ~ 20	m, gm, mg
ls	6 ~ 9	bc
m, gm, mg	mostly > 30 6 ~ 15 on mountains	b
sl, sh	6 ~ 18	m, gm, mg, bc, l

As discussed previously, the thickness of seismic landslides is typically shallow, on the order of several meters. Jibson and Michael (2009) used $t = 15$ m (50 ft) for the seismic landslide hazard maps in Anchorage, Alaska. Such a large thickness was used because $t \leq 15$ m is the typical range of landslide depths observed in Anchorage and it was decided to use the larger value because it leads to smaller k_y and thus is conservative (personal communication, Dr. Randall W. Jibson). In this study, instead of using a large and conservative t value, the epistemic uncertainty in t values is considered.

Shallow landslides usually occur within the surficial weak soils or on the contact surface between the surficial soil and underlying stiff soil/rock. Table 4.5 lists the general thickness of surficial geologic units, and these values are used to estimate reasonable values of t values for the calculation of k_y . The values in Table 4.4 are based on limited information, such that the actual surficial soils may be thinner or thicker across the study area, but these values are the best estimates available and appropriate for regional analysis. Generally, the surficial soil layers are thicker in flat terrain, and thinner in steep terrain. Based on this information and the thicknesses in Table 4.5, the thickness of surficial soils in the landslide-prone units can range from between 3 to 15 m. Thicknesses between 3 to 9 m are considered the most representative for moderate steep to steep slopes because the soil layers should be thinned on steeper slopes. Such estimates are consistent with the engineering observation that landslide depths in Anchorage can extend to a depth of 15 m (Jibson and Michael 2009). The colluvium units (c-br and c-bl) are treated differently based on the thickness estimates shown in Table 4.5. These units are assigned a thickness of 3 m with no uncertainty. The resulting logic-tree for t values is summarized in Table 4.5.

Table 4.5 t values and associated weights in logic-tree analysis

t value (m)	weights for c-br and c-bl	weights for other units
3	1	0.3
6	0	0.4
9	0	0.3

The m value, which is the proportion of the block thickness that is saturated, depends on the groundwater conditions, subsurface hydraulic conductivity, and precipitation, as these parameters influence the groundwater table location. Topography and artesian conditions can cause complicated spatial variations in the ground water table across a region. The estimation of ground water table relies on survey records and average annual precipitation. Jibson et al. (2000) used $m = 0$ to characterize the pore water pressure for slopes in the Oat Mountain quadrangle during the 1994 Northridge earthquake. This value was selected because the coarse-grained surficial slope material was very dry due to no rainfall over the preceding several months, and therefore the groundwater table was below the defined failure depth ($t = 2.4$ m).

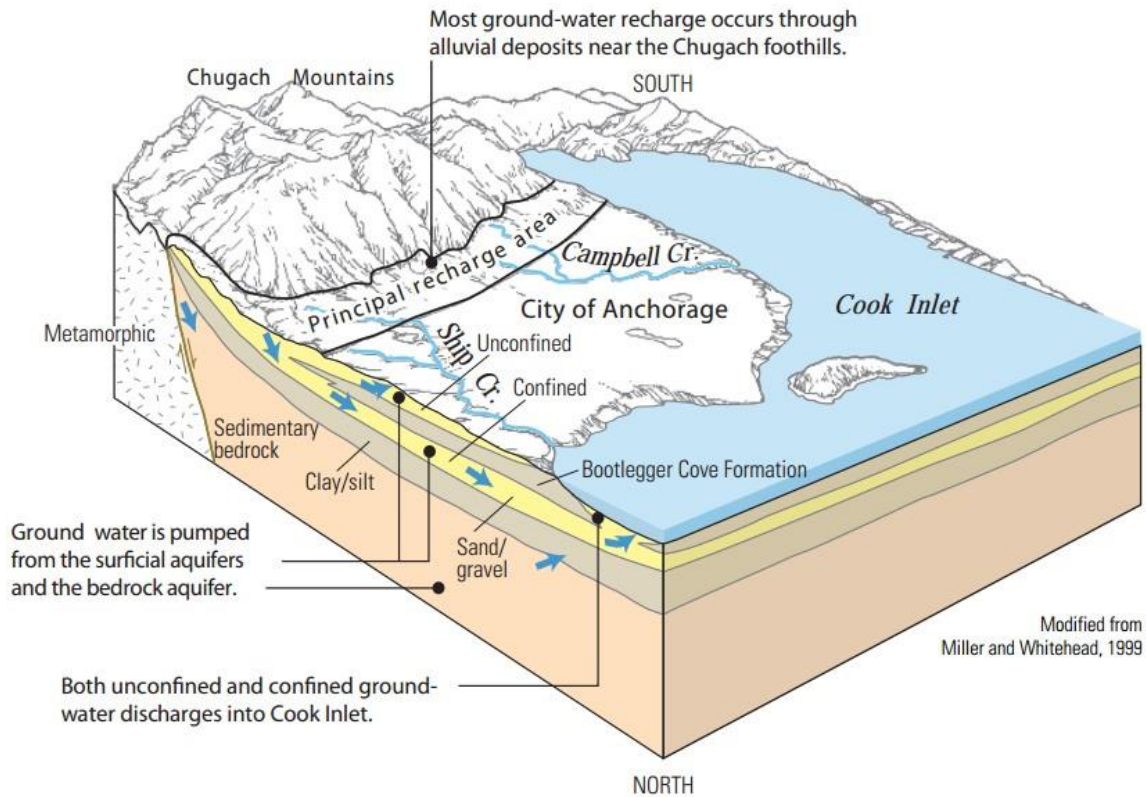


Figure 4.6 Conceptual models of the aquifer systems in Anchorage area (updated by Moran and Galloway, 2006)

The groundwater in Anchorage mostly comes from the Chugach Mountains as illustrated in Figure . In the eastern study area in the foothills of the mountains, the groundwater table should be high because this area is the so-called “Principal recharge area” which is close to the Chugach Mountains. In the central and western study area, slopes along stream valleys and coastal bluffs should also have relatively high groundwater table. Some groundwater data, collected from wells or borings in or around the downtown area, show that the groundwater table is tens of meters below the ground surface, but these data cannot represent the groundwater condition outside the urban area, in which groundwater table is significantly reduced by heavy pumping (Moran and Galloway 2006).

The most commonly observed groundwater table in the Anchorage area is about 3 to 6 m (personal communication, Dr. Randall W. Jibson), and Jibson and Michael (2009) used a 3-m deep groundwater table to calculate their m value. For this study, a uniform distribution is used to simply describe the uncertainty in the groundwater table between 3 and 6 m. We assign 50% probability to the 3-m depth, and another 50% probability to the 6-m depth. The logic tree branches for t and m values are shown in Figure . The two m values associated with each t value represent 3-m depth and 6-m depth groundwater table, respectively. For colluvium units (c-bl and c-br), a constant $t = 3$ m is used, and m is set equal to 0 with the shallowest ground water table at 3 m. Thus, there are not logic tree branches for the colluvium units.

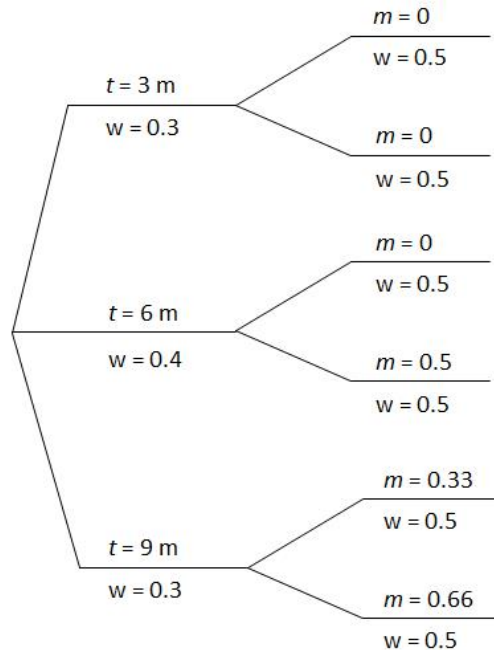


Figure 4.7 Logic tree branches for t and m values for all geologic units except for colluvium units ($t = 3$ m and $m = 0$ for colluvium)

4.3 Ground Motion Characterization for Seismic Landslide Hazard Map

The PGA seismic hazard for Anchorage is obtained from the 2008 National Seismic Hazard Mapping (NSHM) project (<http://geohazards.usgs.gov/hazardtool/>, Petersen et al. 2008). USGS provides a NSHM application through which a PGA hazard curve can be calculated at any location within the United States. Figure shows the PGA hazard curve (solid line) from the 2008 NSHM project for Anchorage (N61.22, W149.90).

The seismic hazard deaggregation data required by Equations 3.4 through 3.7 can also be downloaded from the USGS website. As seen in Figure , the geographic seismic hazard deaggregation presents the spatial distribution of all earthquake sources, providing a more intuitive representation of the seismic hazard deaggregation. The yellow dot, representing the location for which seismic hazard deaggregation is created, is downtown Anchorage. The red line north of Anchorage is the Castle Mountain Fault. The areas enclosed by orange lines at the southeast are megathrust subduction zones, where the northwestward-moving Pacific plate is subducting beneath the North American plate.

These maps show that the deaggregation contributions generally come from two major sources. Much of the hazard comes from earthquake events close to Anchorage, which are shallow crustal events with magnitude generally less than 7.0. Subduction zone events further away also have significant contributions.

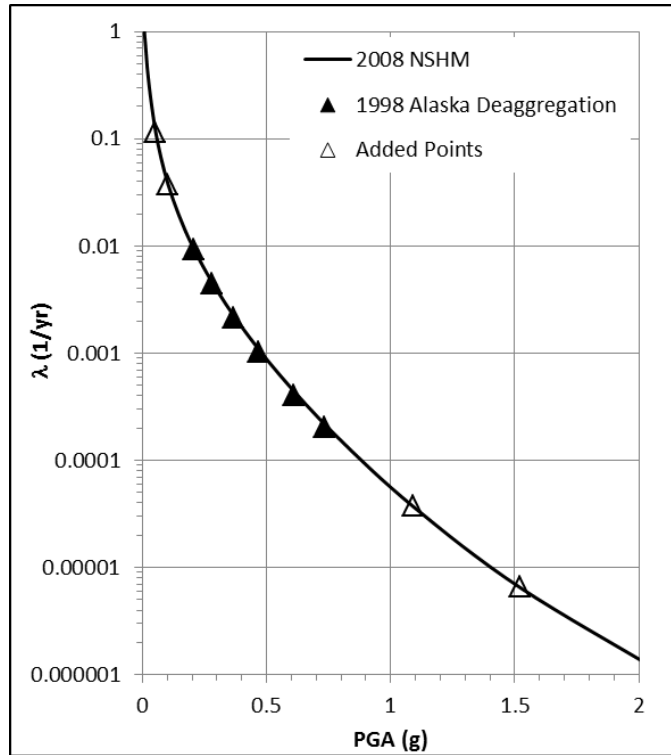
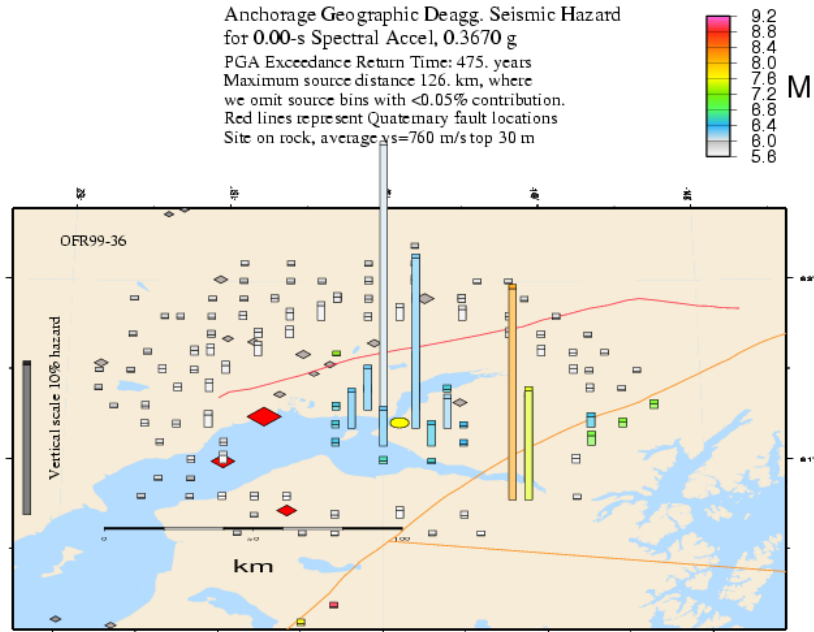


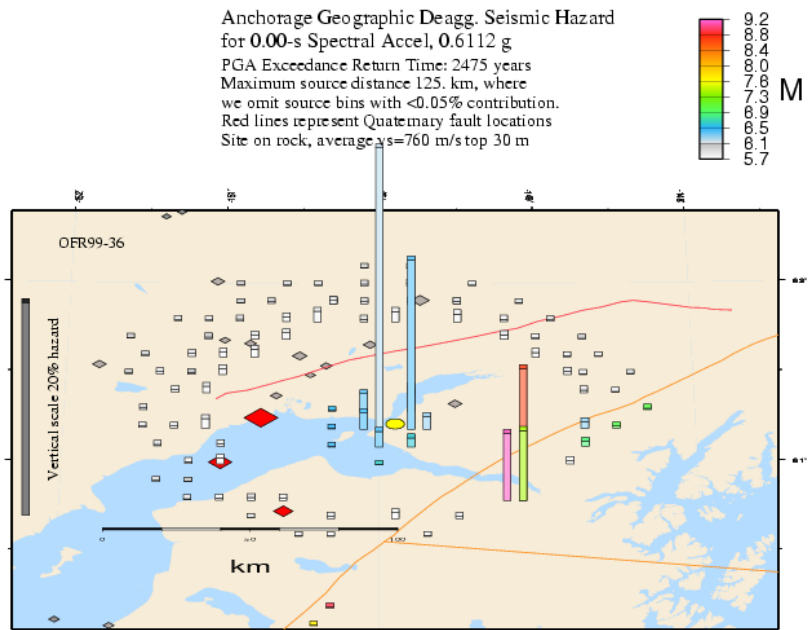
Figure 4.8 PGA Hazard Curve and deaggregation hazard levels for Anchorage (N61.22, W149.90)

The PGA values from the deaggregation are 0.61 g and 0.37 g at 2% and 10% probabilities of exceedance in 50 years, respectively. These PGA levels are smaller than the values used by Jibson and Michael (2009) (i.e., 0.690 g and 0.433g), because the seismic hazard deaggregation for Alaska was published by the USGS in 1998 while Wessen et al. (2007, 2008) updated the PGA seismic hazard in Alaska a decade later without updating the deaggregation. Because the deaggregation information is required to compute the displacement hazard curves, the PGA hazard curve used in the analyses is derived from the PGA values reported in the deaggregation. This maintains consistency between the ground motion values and the deaggregation.

Figure shows the same deaggregation information in terms of percent contribution to the hazard for discrete magnitude and distance bins. The percent contribution represents $P[M_k, R_i | PGA > PGA_i]$, as used in Equations 3.4 through 3.7. Similar to Figure , this deaggregation shows that significant contributions from the hazard come from smaller/closer events and larger/farther events. The binning process sums the contributions of sources within each bin, and assigns the average M and R to that bin. For example, all sources with $M = 6 \sim 6.5$ and $R = 10 \sim 20$ km are combined and their contributions are summed together for this bin. This bin is then assigned a mean magnitude ($M_k = 6.25$) and a mean distance ($R_i = 15$ km). The mean magnitude and distance are 6.74 and 36.7 km for 2% probability of exceedance in 50 years, and 6.66 and 41.7 km for 10% probability of exceedance in 50 years. However, these mean M , R combinations contribute almost nothing to the hazard. The identification of mean M , R scenarios that contribute little hazard occurs when the deaggregation is bi-modal, which is the case in Figure . Because the probabilistic approaches developed in this work incorporate the entire deaggregation, this issue will not be a problem for our analyses.

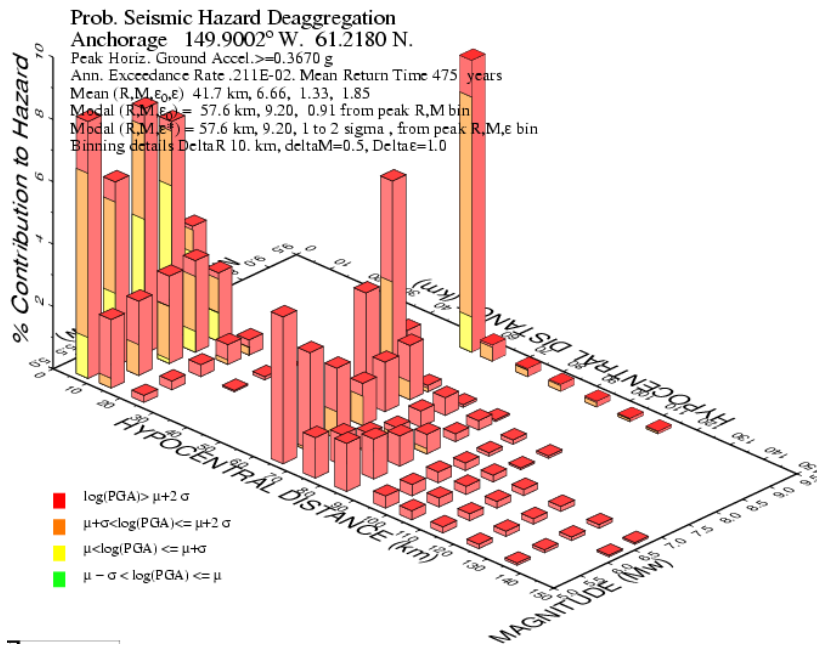


(a)

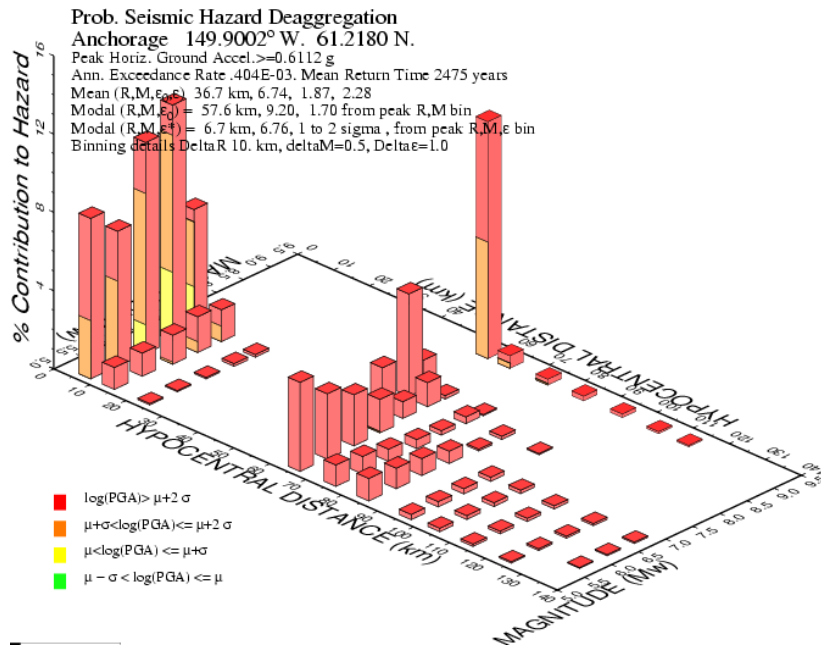


(b)

Figure 4.9 Geographic seismic hazard deaggregation in Alaska at (a) 10% in 50 years and (b) 2% in 50 years



(a)



(b)

Figure 4.10 Seismic hazard deaggregation bins in Anchorage at (a) 10% in 50 years and (b) 2% in 50 years

The USGS published seismic hazard deaggregation data in 1996 for the continental 48 states. In the following decade, two updated versions were published in 2002 and 2008. The 2008 version provides deaggregation data for dozens of seismic hazard levels, but the previous versions only provided deaggregation data for 6 seismic hazard levels. For the State of Alaska, seismic hazard deaggregation data was only published in 1998 and it represents an extension of the 1996 analysis for the continental 48 states. The seismic hazard deaggregation for Alaska was

never updated in 2002 or 2008. Therefore, as shown in Figure , the 1998 Alaska deaggregation only covers a range of hazard levels from 1% probability of exceedance in 50 years ($\lambda = 0.0002$ 1/yr and PGA = 0.73 g) to 50% probability of exceedance in 75 years ($\lambda = 0.009$ 1/yr and PGA = 0.21 g). This range does not represent the entire seismic hazard curve.

The deaggregation information is used to compute $P[M_k, R_1|PGA_i]$ for use in the calculation of the sliding displacement. To deal with the limited amount of deaggregation information, the $P[M_k, R_1|PGA_i]$ for hazard values outside the range available is assumed to be the same as for the closest hazard level. For example, the $P[M_k, R_1|PGA_i]$ for $\lambda < 0.0002$ 1/yr is assigned the values from $\lambda = 0.0002$ 1/yr and the $P[M_k, R_1|PGA_i]$ for $\lambda > 0.009$ 1/yr is assigned the values from $\lambda = 0.009$ 1/yr. Such assumption ignores the tendency that shallow crustal events close to Anchorage have more contributions at smaller λ , while subduction zone events contribute more to the seismic hazard at larger λ . Nonetheless, the associated errors should be small.

As discussed earlier, the vector approach requires the computation of $P[PGV_j|PGA_i]$. This calculation requires ground motion prediction equations (GMPEs) for PGA and PGV. When selecting appropriate GMPEs, the most important issue to consider is the tectonic environment (e.g., active crustal earthquakes vs. subduction earthquakes). The Anchorage study area is complicated by the fact that active crustal events occur close to Anchorage, yet there is also a large subduction zone located as close as 60 to 70 km southeast of the city (Figure). Therefore, GMPEs for both active crustal and subduction events must be used and these two types of earthquakes must be distinguished from each other in the seismic hazard deaggregation data. The distinction of these events and the GMPEs used to model them are described below.

The shallow crustal events around Anchorage typically have magnitudes smaller than 7.0 (Wesson et al. 1999 and 2007) and are mostly within 50 km of the city. Thus, all events closer than 50 km are considered shallow crustal events and all events at distances larger than 50 km are considered subduction events. Subduction events are generally distinguished between intraslab and interface events using the focal depth (Youngs et al. 1997, Kanno et al. 2006). Youngs et al. (1997) summarized that: (1) interface earthquakes are typically shallow (focal depth < 50 km) and occur at the interface between the subducting oceanic plate and overriding continental plate (**Error! Reference source not found.**), and (2) intraslab earthquakes are relatively deeper (focal depth > 50 km) and occur within the subducting oceanic plate. Similarly, Wesson et al. (1999 and 2007) classified subduction zone events with focal depth greater than 50 km as intraslab events, which typically have magnitude smaller than 7.0. They also classified earthquakes with $M > 7.0$ as interface events. There is no focal depth information provided with the deaggregation data, therefore magnitude is used distinguish between intraslab and interface events. Events with magnitudes less than 7.0 and distances greater than 50 km are considered intraslab events and events with magnitudes greater than 7.0 and distances greater than 50 km are considered interface events.

The GMPEs for PGA were selected based on the GMPEs used in the hazard calculations. The USGS open-file report by Wesson et al. (1999) listed the GMPEs used in the 1998 hazard and deaggregation analysis and we selected one shallow crustal GMPE (Boore et al. 1997) and one subduction GMPE (Youngs et al. 1997) from that list for use in this study (Table). The GMPEs for PGV was selected based on the currently availability relationships. The Boore and Atkinson (2008) GMPE for PGV was selected for shallow crustal events because it is the most simply of the Next Generation Attenuation (NGA) relationships. The availability of a PGV GMPEs for subduction zone events is very limited, because PGV was not considered an important ground motion parameter until relatively recently. The most recent GMPE for PGV

for subduction zone events was developed by Kanno et al. (2006) using ground motion data in Japan and this relationship is used in this study (Table).

Table 4.6 GMPEs for PGA and PGV in Anchorage

Seismic event categories	PGA GMPEs	PGV GMPEs	Distance metrics
R<50 km Shallow Crustal Events	BJF97	BA08	R _{JB}
R>50 km, M<7 Subduction Intraslab Events	Youngs97	Kanno06	R _{rup}
R>50 km, M>7 Subduction Interface Events	Youngs97	Kanno06	R _{rup}

The correlation coefficient between PGA and PGV also is required in the vector hazard calculation. The correlation coefficient between PGA and PGV has been estimated as 0.6 (Rathje and Saygili 2008, Baker 2007). Thus, the joint probability $P[PGA_i, PGV_j]$ can be calculated for the vector approach, as shown in Figure . Generally, pairs of larger PGA and PGV have smaller annual probabilities of occurrence, while pairs of smaller PGA and PGV have larger probabilities. In addition, the probability of a small PGA occurring with a large PGV is very small, and vice versa.

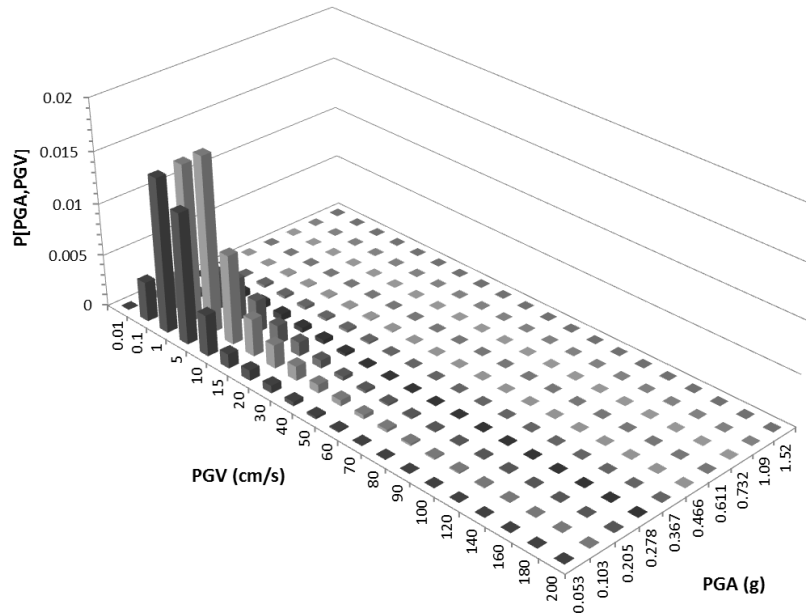


Figure 4.11 Joint annual probabilities of occurrence for (PGA, PGV) pairs

4.4 Logic Tree

To incorporate the epistemic uncertainties into the seismic landslide hazard mapping, a logic-tree analysis is applied to the various sources of uncertainties. The logic tree is separated into three parts, representing epistemic uncertainties in shear strength, slope properties, and displacement prediction models. The logic tree is shown in Figure and its components are explained below.

Part 1 of the logic tree shows possible combinations of shear strengths and associated weights. Best estimate properties (c_{best} and ϕ_{best}) as well as high (c^+ and ϕ^+) and low (c^- and ϕ^-) values were assigned to each geologic unit based on the discussion in Section 4.2. The best estimates of shear strength for all geologic units are shown in

Table 4.3. The undrained shear strength has a coefficient of variation (COV) equal to 30%, and the effective friction angle has a COV equal to 10%. The COV for effective cohesion is assumed to be 20% so that the total uncertainty in drained shear strength is similar to undrained shear strength. Therefore, for those geologic units with $\phi = 0$, the cohesion assigned as an undrained shear strength varies +/-39% (i.e., +/-1.3·COV) above/below (c^+/c^-) the best estimate value. For those units with drained shear strengths, the effective friction angle is varied +/-13% based on its COV, and the effective cohesion has is varied +/-26% based on its COV. The weights are assigned first to friction angle as: (1) 0.4 to the best estimate and (2) 0.3 to the values above/below the best estimates as shown in Table 4.4. When assigning weights to the associated cohesion values, it is considered that the combinations of (c^+, ϕ^+) or (c^-, ϕ^-) are less likely than (c^+, ϕ^-) or (c^-, ϕ^+). Therefore, the weights for cohesion values associated with (c^+, ϕ^+) or (c^-, ϕ^-) are taken as 0.25 and the weights for cohesion values associated with (c^+, ϕ^-) or (c^-, ϕ^+) are taken as 0.35. The weight for the cohesion values associated with (c_{best}, ϕ_{best}) is equal to 0.4.

The epistemic uncertainties for the t and m values are presented in Part 2 of the logic tree. The best estimate t value is 6 m for all geologic units except the colluvium units of c-br and c-bl. Additional values of 3 m and 9 m are selected to represent the potential range of landslide depths across Anchorage, and the associated weights are 0.3, 0.4 and 0.3 as noted in Section 4.2. Because the colluvium units (c-br and c-bl units) exist on the surface of slopes as a thin layer, their depths were assumed as 3 m, and no variability was considered in the logic-tree analysis. Two groundwater depths (i.e. 3 m and 6 m) are selected to calculate m values for each of the t values. For example, if the t value is 6 m, the two corresponding m values are 0 and 0.5 for the different groundwater depths. The two m values for each t value are equally weighted.

The first two parts of the logic tree are related to the calculation of the yield acceleration using the infinite slope model. The different branches result in 56 different values of k_y and corresponding weights associated with each grid cell. These 56 values of k_y will be used to define the mean displacement hazard curve.

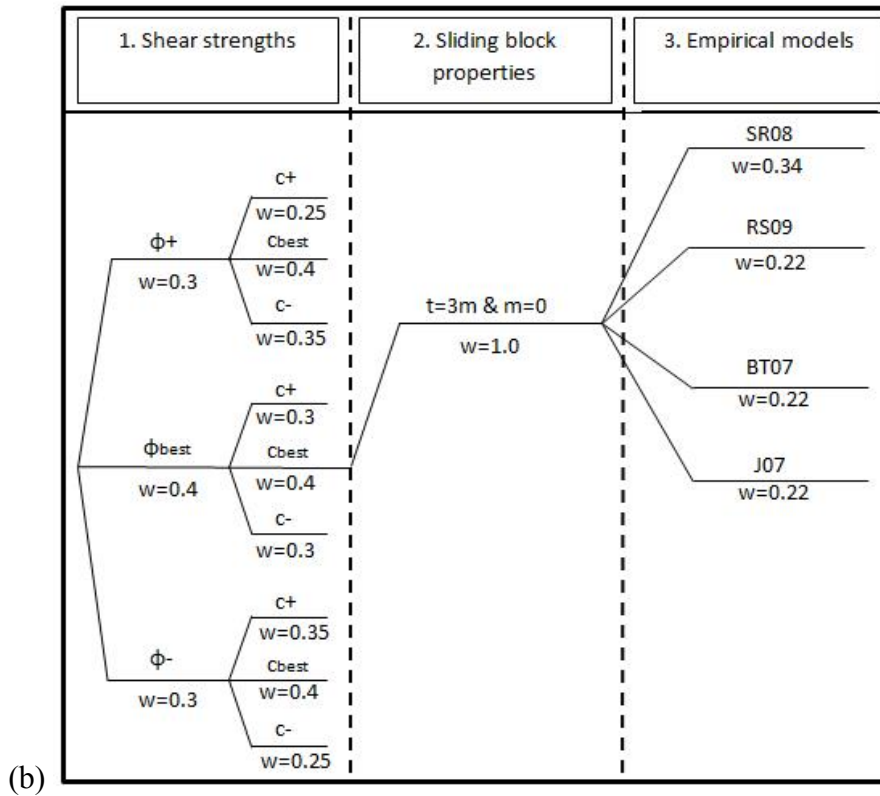
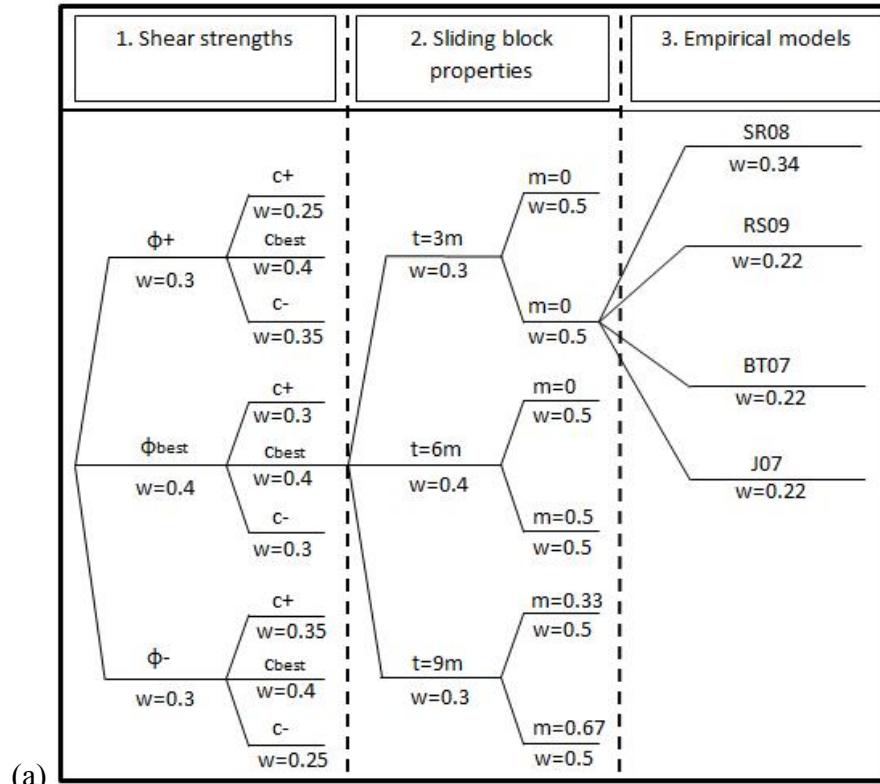


Figure 4.12 Logic tree with weights for (a) geologic units (except colluvium units), and (b) colluvium units (c-bl and c-br)

Finally, the epistemic uncertainty associated with the different empirical displacement models is incorporated in Part 3 of the logic tree. Three scalar models that use PGA and earthquake magnitude are selected for use (Rathje and Saygili 2009, Jibson 2007, Bray and Travararou 2007), as well as one vector model that uses PGA and PGV (Saygili and Rathje 2008). These models are labeled RS09, J07, BT07, and SR08. Figure shows the predicted sliding displacements as a function of k_y/PGA for the four empirical models for $M = 6.74$, $PGA = 0.61$ g, and $PGV = 34$ cm/s. The PGA and M values come directly from the hazard information for Anchorage, while the PGV represents the conditional value given $PGA = 0.61$ g and correlation coefficient $\rho_{PGA,PGV} = 0.6$. The four empirical models in Figure predict displacements that vary by a factor of about 4 for this scenario. For other scenarios there may be more or less difference between these models. Such difference is the epistemic uncertainty to be captured. To assign the weights, the scalar models are equally weighted at 0.22 and the vector model is weighted at 0.34. The vector model is more heavily weighted because the use of a second ground motion parameter provides a better estimate of sliding displacement.

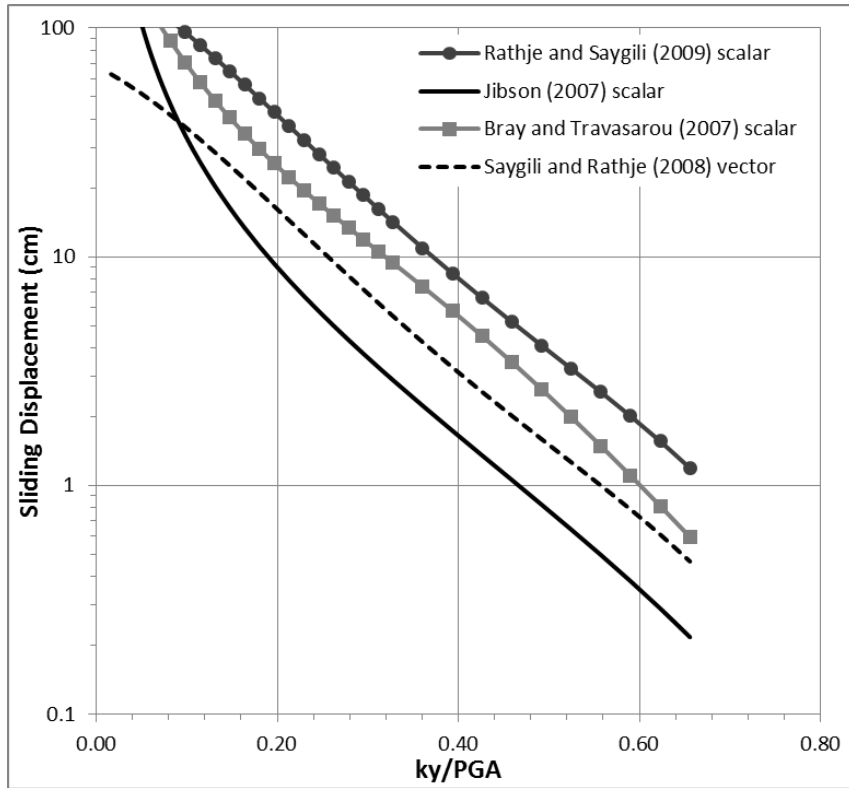


Figure 4.13 Comparison of Predictive Models for a scenario of $M = 6.74$, $PGA = 0.61$ g and $PGV = 34$ cm/s

4.5 Regression Models and Screening Analysis

The Mean λ_D Threshold approach to applying the logic tree analysis on a regional scale requires an interpolation relationship between k_y and $\lambda_D(x)$, which can be expressed as a 4th order polynomial regression model in the form of:

$$\ln(\lambda_D(x)) = a_1(\ln(k_y))^4 + a_2(\ln(k_y))^3 + a_3(\ln(k_y))^2 + a_4\ln(k_y) + a_5 \quad (4.7)$$

The regression relationship is specific to a specified ground motion hazard, a specified level of displacement x , and a specified empirical displacement model. The coefficients used in Equation 4.1 are provided in Table for the Anchorage ground motion hazard, three displacement thresholds, and the four empirical displacement models considered. The three displacement thresholds (1 cm, 5 cm and 15 cm) represent moderate, high and very high seismic landslide hazard categories (Table **Error! No text of specified style in document..1**).

With these regression models and Equation 4.1, the mean annual rate of exceedance for a specific displacement threshold ($\overline{\lambda_D}(x)$, where x is the displacement threshold) at each grid cell can be computed from the 216 branches in the logic tree and the associated weights. After comparing the computed $\overline{\lambda_D}(x)$ with the hazard level under consideration (λ^*), the seismic landslide hazard category of each grid cell can be determined.

Table 4.7 Coefficients of regression models

Displacement Threshold	Empirical Displacement Models		a_1	a_2	a_3	a_4	a_5
1 cm	Scalar	RS09	0.0067	0.0673	-0.2122	-3.5961	-10.7348
		J07	0.0089	0.1051	-0.0672	-3.7699	-11.8035
		BT07	0.0116	0.1377	0.0984	-3.2727	-11.0939
	Vector	SR08	-0.0024	-0.0088	-0.3859	-3.7557	-11.4605
5 cm	Scalar	RS09	0.0044	0.0529	-0.1717	-3.4082	-11.3582
		J07	-0.0013	0.0061	-0.3379	-4.1157	-13.0937
		BT07	-0.0036	-0.0161	-0.3892	-3.9692	-12.2431
	Vector	SR08	-0.0139	-0.1396	-0.8389	-4.3842	-12.7071
15 cm	Scalar	RS09	-0.0029	-0.0212	-0.3917	-3.6514	-12.1558
		J07	-0.0224	-0.2211	-1.1387	-5.3158	-14.6797
		BT07	-0.0512	-0.5404	-2.35	-7.037	-15.0673
	Vector	SR08	-0.0397	-0.4348	-2.0095	-6.3164	-14.6476

To further reduce the computation time, a screening analysis is performed first using the worse-case scenario of the logic tree. The lowest shear strengths (c^- and ϕ^-) and the largest m and t values (0.67 and 9 m for drained units, 0 and 3 m for undrained units) are used to compute the minimum factor of safety for each grid cell. The RS09 scalar model is selected for the screening analysis because it generally predicts the largest sliding displacement relative to the other three models, as seen in Figure . All grid cells in which $\lambda_D(5\text{cm})$ is greater than $\lambda^* = 0.0004$ 1/yr (i.e., 2% probability of exceedance in 50 years) are colored red in Figure . All non-

red grid cells are excluded from the full logic-tree analysis for a hazard level greater than 2% in 50 years, because these grid cells do not have landslide potential for the 5-cm threshold even under the worst-case condition. Similar screening analysis is carried out for the 1-cm and 15-cm thresholds.

For the 5-cm threshold, only 9.0% of grid cells in the study area are colored red, which means that about 91% of the study area is removed from the full logic-tree analysis. For the 1-cm and 15-cm thresholds, about 73% and 95% of study area is removed from analysis by applying the screening analysis first. Therefore, the full logic-tree analysis for a specified displacement threshold performed using Python codes in ArcGIS® can be completed within an hour for the Anchorage study area.

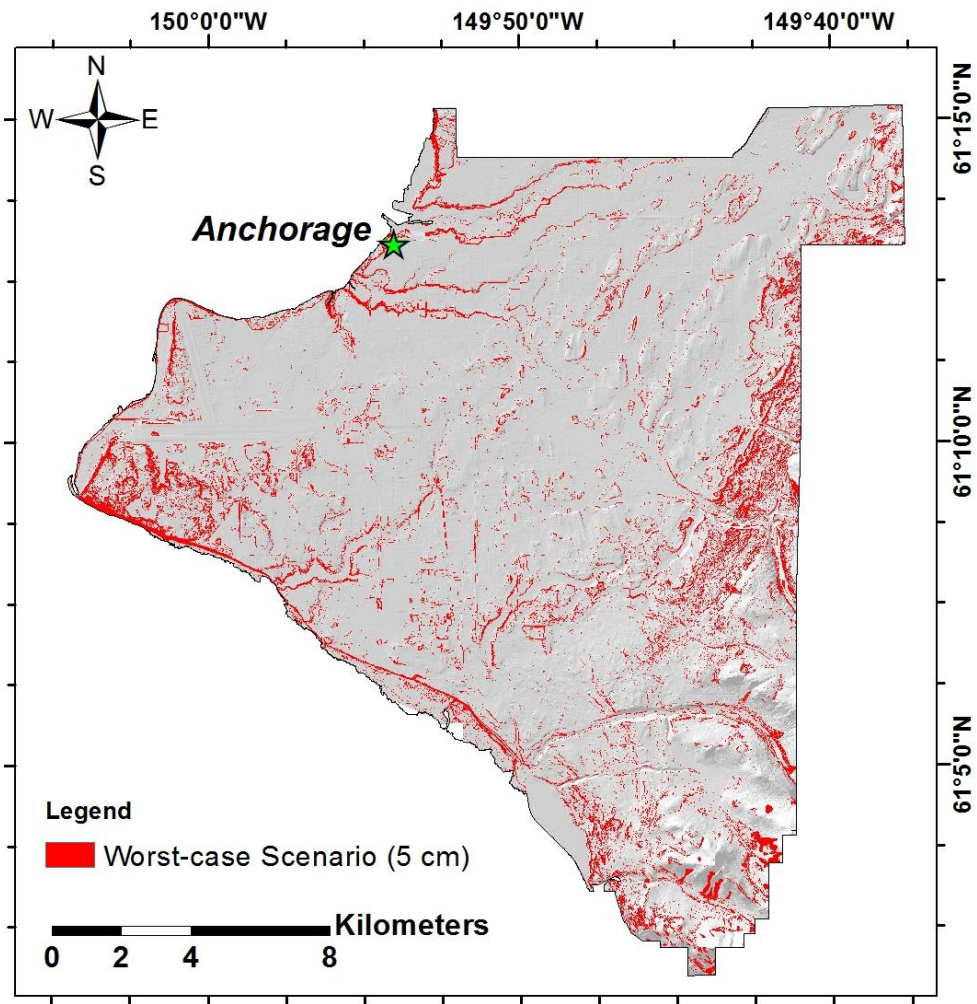


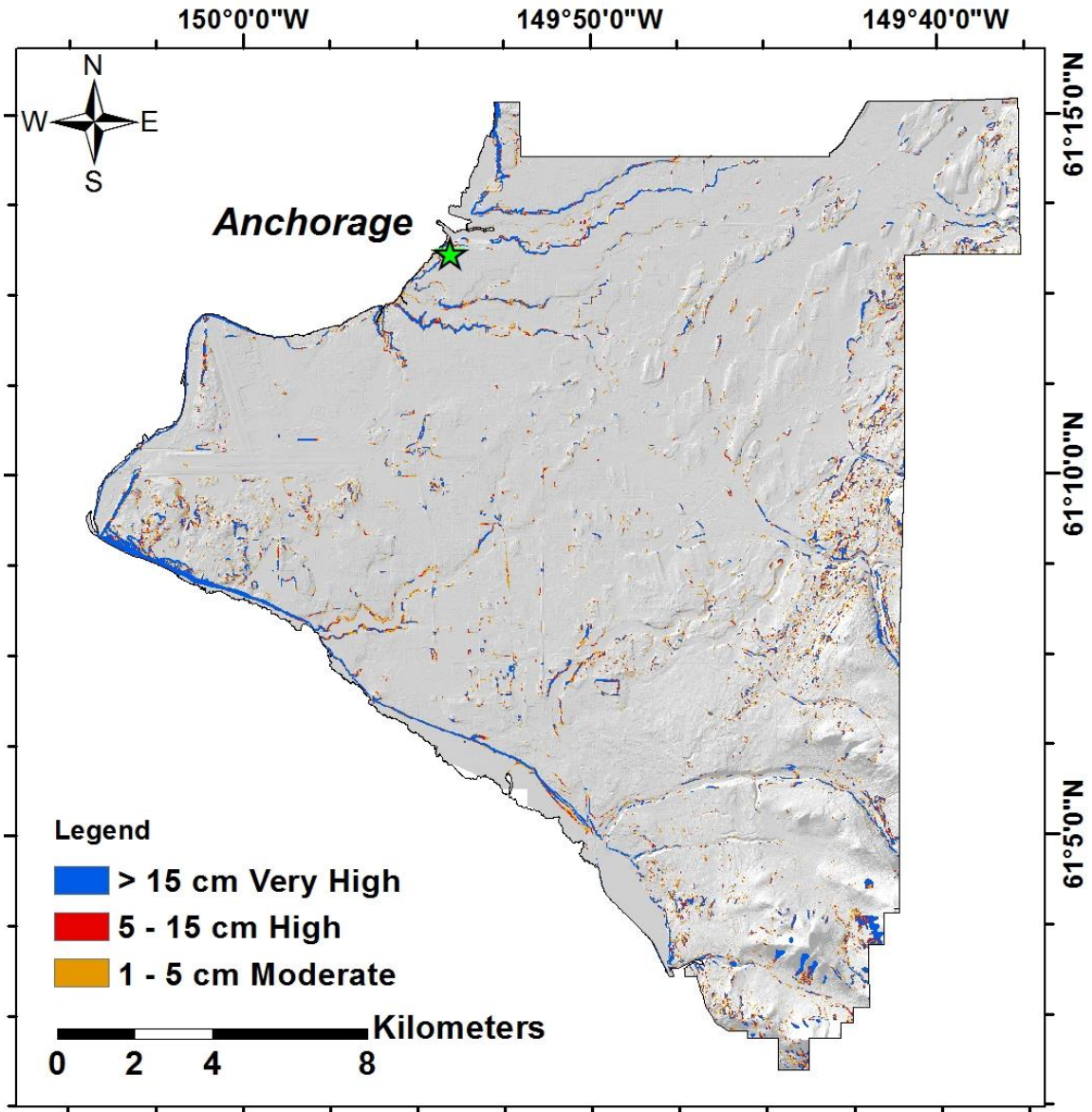
Figure 4.14 Cells with $\lambda_D(5\text{cm}) > 0.0004$ 1/yr for worst-case condition (5-cm threshold, 2% in 50 years)

4.6 Results

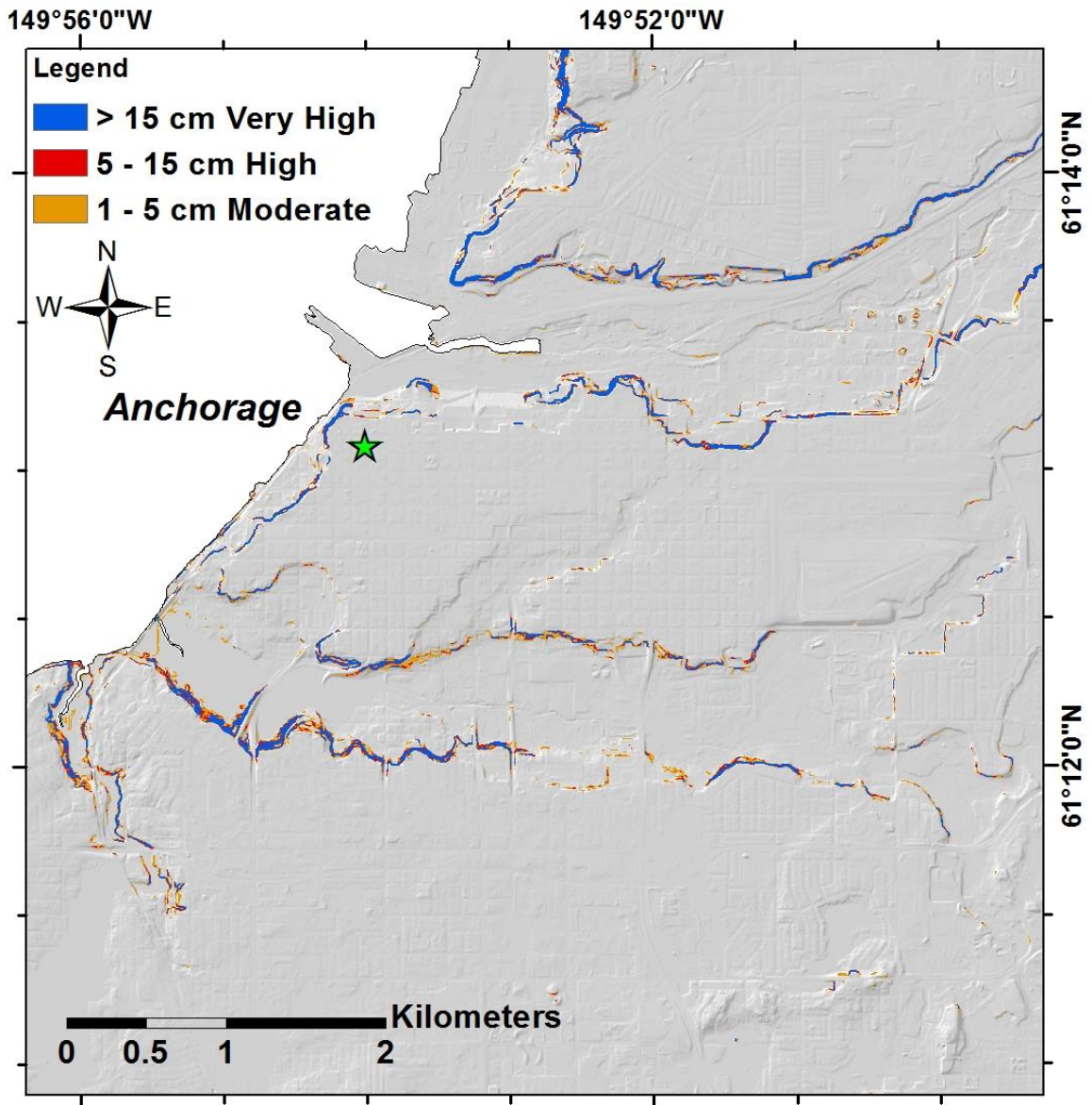
Using the procedures described above, a probabilistic seismic landslide hazard map was created by running Python codes in ArcGIS®. **Error! Reference source not found.** plots such a hazard map of the Anchorage study area for a 2% probability of exceedance in 50 years ($\lambda^* = 0.0004$ 1/yr) and the three seismic landslide categories (moderate, high, and very high). The area with moderate hazard ($1 \text{ cm} < D < 5 \text{ cm}$, colored orange) and high hazard ($5 \text{ cm} < D < 15 \text{ cm}$, colored red) are about 0.85% and 0.33% of the entire study area respectively, and the area with very high hazard ($D > 15 \text{ cm}$, colored blue) covers 0.96% of the entire study area. These results cannot be compared directly with the current deterministic map developed by Jibson and Michael (2009) because the deterministic map assumed a worst-case scenario ($t = 15 \text{ m}$ and $m = 0.8$).

As seen on the map, most areas with high or very high hazard are along coastal bluffs, stream valleys or in mountainous areas. More detailed landslide predictions are shown on **Error! Reference source not found.** for downtown Anchorage, located between Ship Creek to the north and Chester Creek on the south. Colluvium and landslide deposits on slopes along coastal bluffs and stream valleys are most susceptible to seismic landslides around the downtown area. **Error! Reference source not found.** plots the seismic landslide hazard for a 10% probability of exceedance in 50 years ($\lambda^* = 0.0021$ 1/yr). The area with moderate, high and very high hazard are about 0.18%, 0.14% and 0.60% of the entire study area, respectively. The seismic landslide hazard at this smaller hazard level is significantly reduced across the study area, except for the c-bl unit along coastal bluffs and stream valleys.

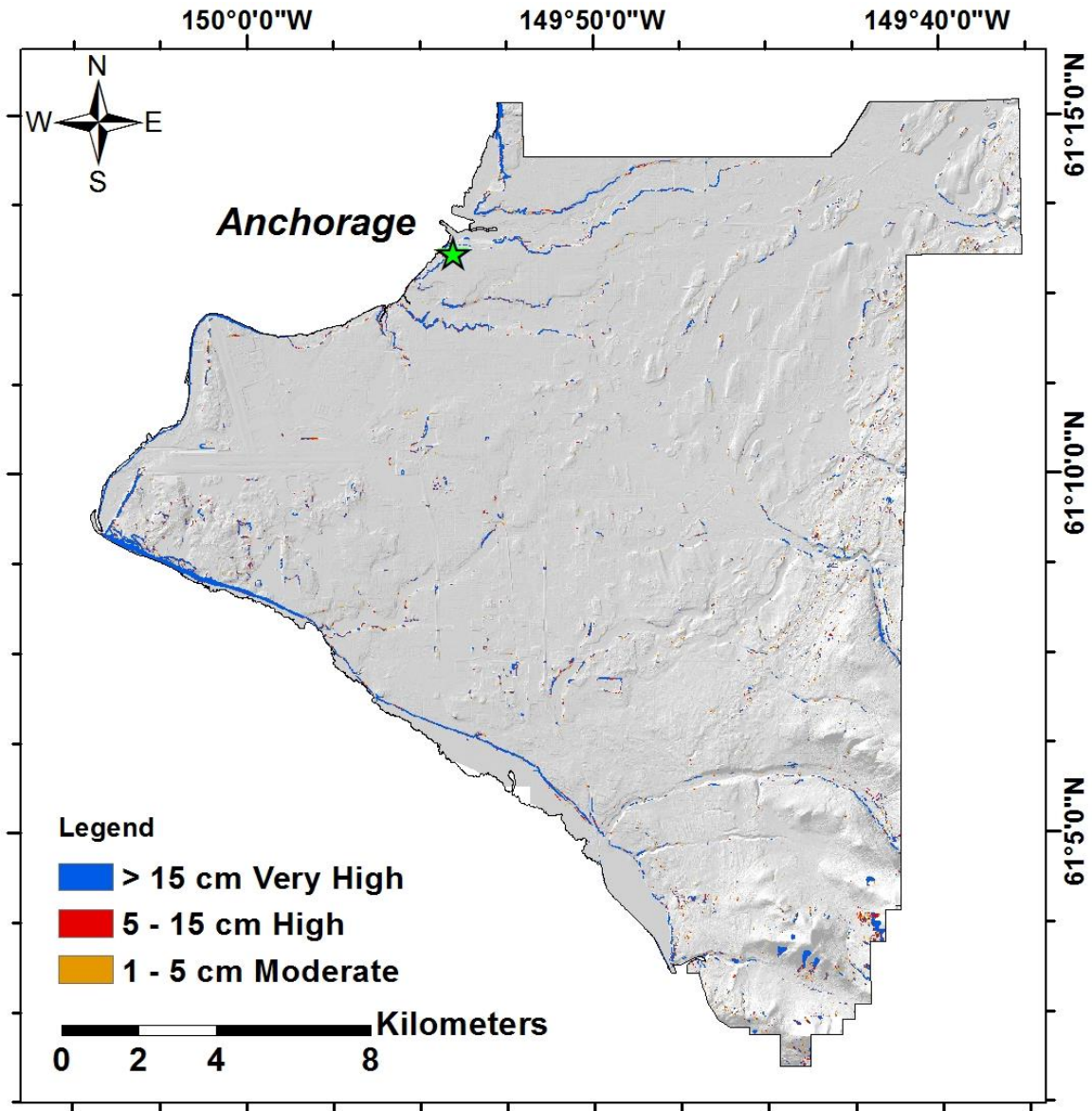
To investigate the influence of each part of the logic tree on the seismic landslide hazard, a series of displacement maps were created by implementing different parts of the logic tree (i.e., epistemic uncertainty). Also analyzed is the deterministic approach in which the 2% in 50 year PGA was used to compute sliding displacements. This deterministic approach is essentially the approach used by Jibson and Michael (2009), although with different assumed slope properties.



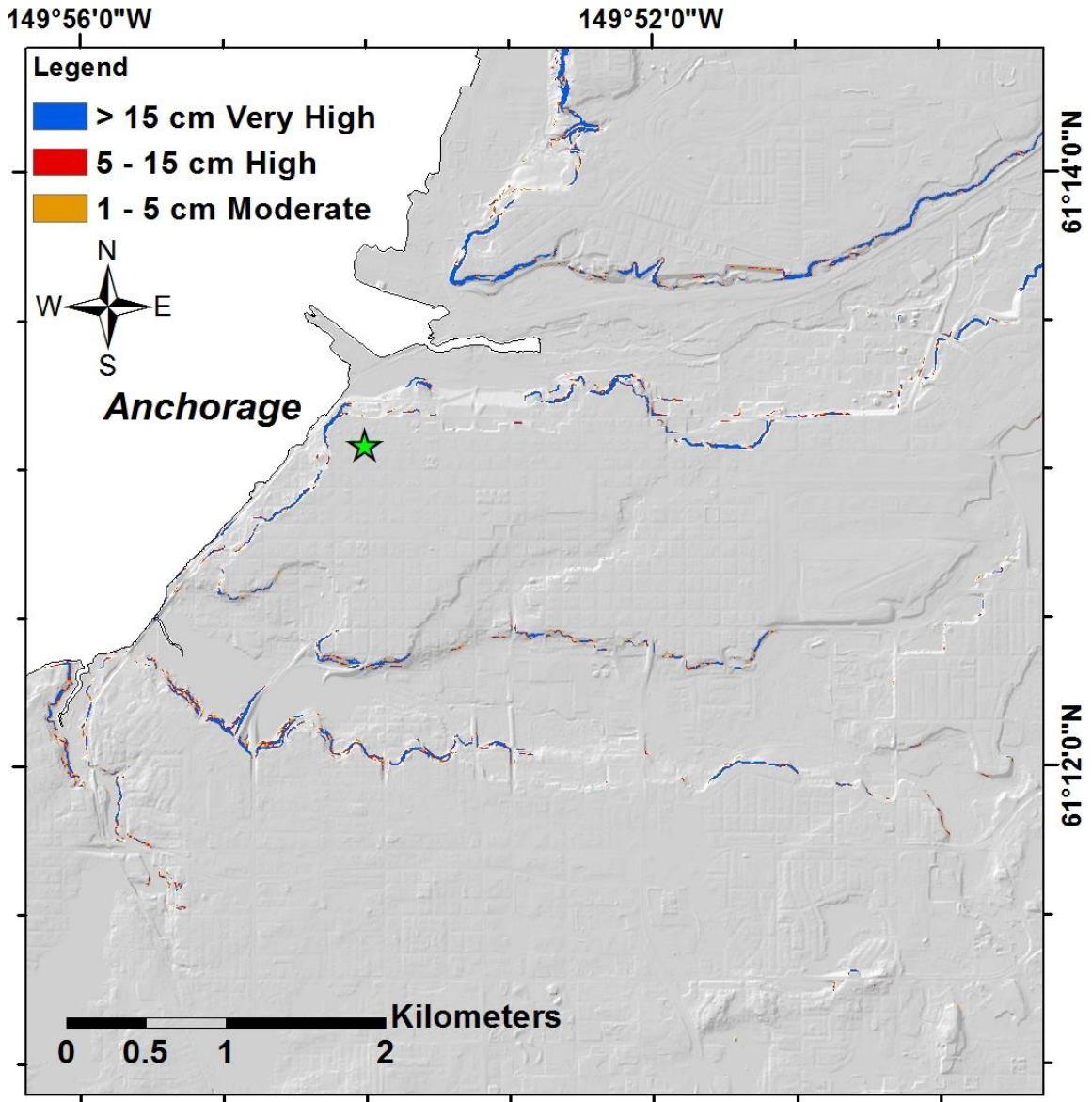
Error! Reference source not found. Probabilistic seismic landslide hazard map of Anchorage study area at 2% probability of exceedance in 50 years



Error! Reference source not found. Probabilistic seismic landslide hazard map of downtown Anchorage at 2% probability of exceedance in 50 years



Error! Reference source not found. Probabilistic seismic landslide hazard map of Anchorage study area at 10% probability of exceedance in 50 years



Error! Reference source not found. Probabilistic seismic landslide hazard map of downtown Anchorage at 10% probability of exceedance in 50 years

The percentage of the study area exceeding different displacement thresholds when incorporating different parts of the logic tree is summarized in Table . Ten different cases are shown. Cases 1 to 5 only use one empirical displacement model (RS09 scalar model), while all four models are applied to Cases 6 to 10. The deterministic cases (Cases 1 and 6) use the best estimates of all slope properties for the k_y computation. The probabilistic cases (Cases 2-5, 7-10) all incorporate aleatory variability but different components of epistemic uncertainty.

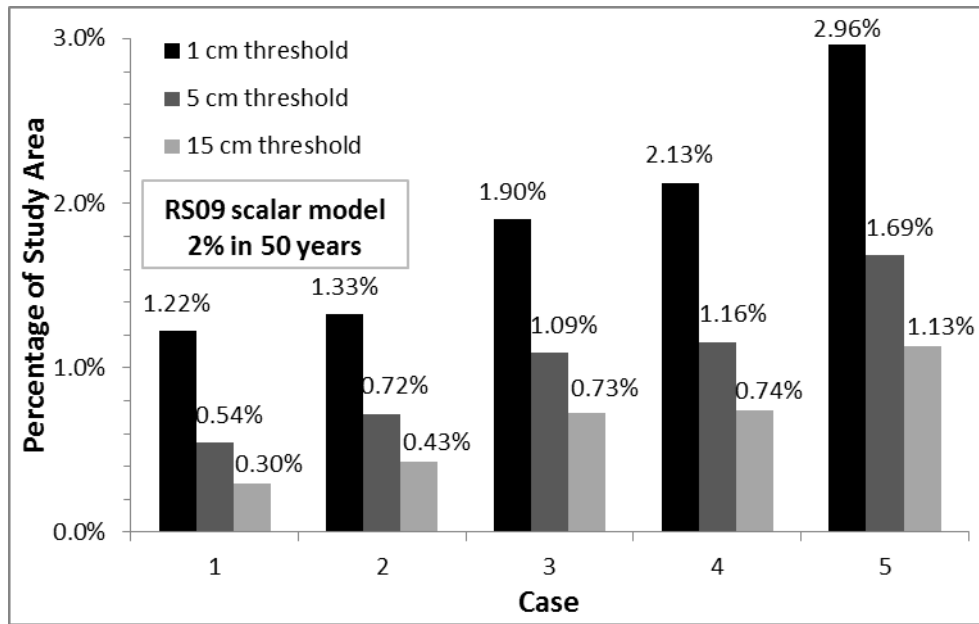
The results in Table are summarized in Figure for the RS09 model. The area of high/very high hazard (i.e., $D > 5$ cm) increases by 33% when aleatory variability is included (i.e., 0.72% for Case 2 vs. 0.54% for Case 1), and increases by more than a factor of 3 when all of the sources of epistemic uncertainty in k_y are included (i.e., 1.69% for Case 5 vs. 0.54% for Case 1). The influence of the epistemic uncertainty in the sliding block properties (Case 4) is generally greater than the influence of the epistemic uncertainty in the shear strengths (Case 3) because the uncertainties in m and t are larger than the uncertainties in c and ϕ (Figure). However, the difference between these two sources of uncertainty is smaller at larger displacement thresholds. The reason is that the c-bl unit is not assigned uncertainties in t and m values (Figure) and this geologic unit contributes significantly to the landslide hazard in the very high hazard category.

The combined influence of the epistemic uncertainties in the shear strength and sliding block properties (Case 5) is slightly greater than the simple summation of individual influences (Cases 3 and 4), indicating that the combined effect of uncertainties may amplify the increase in the seismic landslide hazard. The same trend is observed for 1 cm and 15 cm thresholds.

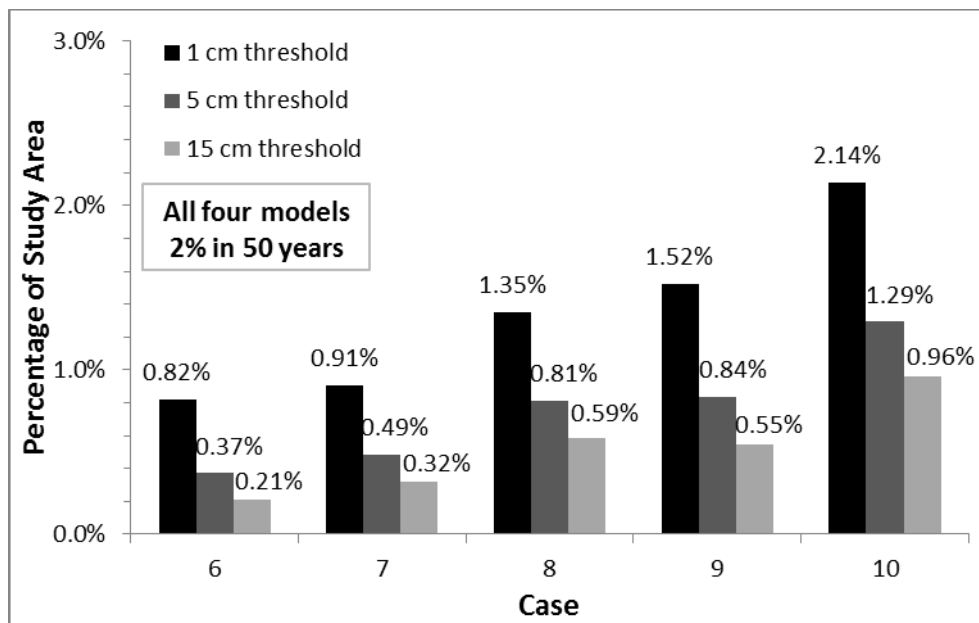
The analyses using all four empirical displacement models (Figure 4.19b) always predict less area within each seismic landslide hazard level than the corresponding analyses using the RS09 model (Figure 4.19a). This difference is a result of the RS09 model generally predicting the largest sliding displacements among all four models (Figure).

Table 4.8 Implementing different parts of the logic tree (2% in 50 years)

Case	Aleatory Variability	Epistemic Uncertainty	% of Study Area			
			$D > 1$ cm	$D > 5$ cm	$D > 15$ cm	
RS09 scalar model	1	No	No	1.22%	0.54%	0.30%
	2	Yes	No	1.33%	0.72%	0.43%
	3	Yes	Shear Strength	1.90%	1.09%	0.73%
	4	Yes	Sliding Block	2.13%	1.16%	0.74%
	5	Yes	Shear Strength and Sliding Block	2.96%	1.69%	1.13%
All four models	6	No	No	0.82%	0.37%	0.21%
	7	Yes	No	0.91%	0.49%	0.32%
	8	Yes	Shear Strength	1.35%	0.81%	0.59%
	9	Yes	Sliding Block	1.52%	0.84%	0.55%
	10	Yes	Shear Strength and Sliding Block	2.14%	1.29%	0.96%



(a)



(b)

Figure 4.19 The influence of different parts of the logic tree on the computed seismic landslide hazard at 2% probability of exceedance in 50 years using (a) RS09 scalar model and (b) all four empirical displacement models

To investigate the hazard distribution among geologic units, the number of grid cells with high/very high hazard ($D > 5$ cm) in each geologic unit is summarized and shown in Table . Landslide Cells are grid cells with predicted displacements greater than the 5-cm threshold, the % of Study Area represents the percentage of the study area covered by each geologic unit, the % of Geo Unit is the percentage of grid cells with $D > 5$ cm for each geologic unit, and the % of Landslide Cells is the contribution of each geologic unit to all landslide cells in the study area. Also shown in Table 4.9 are the corresponding values from the Jibson and Michael (2009) map.

With 35% of its area predicted as high/very high hazard, the colluvium unit c-bl is most susceptible to landslides, because this unit has low undrained shear strength and mostly covers steep coastal bluffs and valley walls (Figure 4.5). Landslide deposits (ls), mostly distributed on coastal bluffs, valley walls and the Chugach Mountains, also has a large portion of its area (about 15%) classified as high/very high hazard. Glacial alluvium (ga) and sand deposits (sh) in low hills, both having more than 2.5% of their area with $D > 5$ cm, also contribute to the landslide hazard. Although the alluvium units, af and al, contribute more than 20% of all landslide cells (each about 10%), they are relatively stable because only 1.1% and 0.6% of these units are classified as high/very high hazard. The only reason these units contribute so much to the overall landslide hazard is because they cover a large percentage of the study area. The other geologic units, which either have high shear strength underlain by stiff soil/rock (e.g. m, gm and mg) or exist mostly on flat terrain (e.g. an, f and l), do not represent a significant seismic landslide risk.

Table 4.9 also summarizes the results from the Jibson and Michael (2009) deterministic map that uses the 2% in 50 year ground motions. The colluvium unit in the mountainous area (c-br) was predicted as one of the most landslide-susceptible unit in the Jibson and Michael (2009) deterministic map, but it has almost no seismic landslide hazard according to the probabilistic analysis. The use of conservative sliding block properties in the deterministic map leads to an over-prediction in the landslide hazard for this unit. In fact, the conservative sliding block properties used by Jobson and Michael (2009) resulted in a much larger area of seismic landslide hazard than predicted in this study. This result demonstrates that is may be more useful to use a logic-tree approach to assign a range of possible model parameters rather than using conservative parameters.

Table 4.9 Distribution of predicted landslides across geologic units (5 cm threshold, 2% probability of exceedance in 50 years)

Geo Units	This Study			Jibson and Michael (2009)		
	Landslide Cells	% of Study Area	% of Geo Unit	% of Landslide Cells	% of Geo Unit	% of Landslide Cells
af	10486	11.4%	1.1%	9.7%	2.2%	6.1%
al	11327	22.0%	0.6%	10.5%	1.3%	7.0%
an	2536	9.8%	0.3%	2.3%	0.6%	1.4%
b	18	2.2%	0.0%	0.0%	0.4%	0.2%
bc	3071	2.8%	1.3%	2.8%	1.9%	1.2%
c-br	65	6.1%	<0.1%	0.1%	18.9%	27.4%
c-bl	36796	1.3%	34.7%	34.0%	93.0%	28.2%
f	362	3.0%	0.1%	0.3%	0.7%	0.5%
ga	11535	5.3%	2.6%	10.7%	7.7%	9.6%
gm	491	3.9%	0.2%	0.5%	0.9%	0.8%
l	471	1.8%	0.3%	0.4%	0.7%	0.3%
ls	13061	1.0%	15.0%	12.1%	22.4%	5.6%
m	3262	6.0%	0.7%	3.0%	3.0%	4.2%
mg	1666	9.5%	0.2%	1.5%	0.8%	1.8%
s	2966	2.0%	1.8%	2.7%	2.8%	1.4%
sh	7404	2.1%	4.2%	6.8%	5.8%	3.0%
sl	2626	10.0%	0.3%	2.4%	0.5%	1.3%
Total	108143	100.0%		100.0%		

5.0 CONCLUSIONS

Current practice uses a deterministic approach to predict the seismic sliding displacement of slopes and to develop seismic landslide hazard maps. The deterministic approach ignores the aleatory variability in the predictions of ground shaking and displacements, as well as the epistemic uncertainties in the slope properties. A probabilistic framework was described that computes a displacement hazard curve using: (1) a ground motion hazard curve from a probabilistic seismic hazard analysis, (2) a model for predicting the sliding displacement of the sliding mass, and (3) a logic tree analysis that incorporates the uncertainties in the various input parameters. This probabilistic framework was applied to regional analysis for seismic landslide mapping around the Anchorage, Alaska area. For this application, the ground motion hazard was derived from the seismic hazard data from the USGS and the logic-tree was derived from available field/laboratory data and engineering judgment.

The resulting seismic landslide hazard maps for Anchorage indicated that 1.29% of the study area has high or very high seismic landslide hazard (i.e., displacements greater than 5 cm) at 2% probability of exceedance in 50 years. At 10% probability of exceedance in 50 years the high/very high seismic landslide hazard areas represents 0.74% of the study area. Most of the areas with high or very high hazard are along coastal bluffs, stream valleys or in mountainous areas. The probabilistic map that includes aleatory variability and epistemic uncertainties identified the area with high/very high hazard that is 3 times larger than identified through the deterministic approach. The influence of the epistemic uncertainty in the sliding block properties on the computed displacements is generally greater than the influence of the epistemic uncertainty in the shear strengths because the uncertainties in sliding block properties are larger than the uncertainties in shear strength. The combined influence of the epistemic uncertainties in the shear strength and sliding block properties is slightly greater than the simple summation of individual influences, indicating that the combined effect of uncertainties may amplify the increase in the seismic landslide hazard. Finally, comparison with a previous deterministic seismic landslide map developed by the USGS indicates that the seismic landslide hazard from the probabilistic analyses is smaller because the deterministic map used very conservative assumptions with respect to the sliding block properties. This comparison indicates that the logic-tree approach provides an alternative way to rigorously account for uncertainties in slope properties, and it can avoid using overly conservative input parameters to capture these uncertainties in a deterministic approach.

REFERENCES

- Baker, J. W. (2007). Correlation of ground motion intensity parameters used for predicting structural and geotechnical response. 10th international conference on applications of statistics and probability in civil engineering. Tokyo, Japan.
- Bazzurro, P. and Cornell, C. A. (2002). Vector-valued probabilistic seismic hazard analysis. Proceedings, 7th U.S. National Conference on Earthquake Engineering, Boston, MA. 10 p.
- Boore, D. M. and Atkinson, G. M. (2008). Ground-motion prediction equations for the average horizontal component of PGA, PGV, and 5%-damped PSA at spectral periods between 0.01 s and 10.0 s. *Earthquake Spectra*, 24(1), 99–138.
- Boore, D. M., Joyner, W., and Fumal T. (1997). Equations for estimating horizontal response spectra and peak acceleration from Western North American earthquakes—a summary of recent work. *Seismological Research Letters*, 68(1), 128–153.
- Bradley, B. A. (2010). A generalized conditional intensity measure approach and holistic ground motion selection. *Earthquake Engineering and Structural Dynamics*, 39(12), 1321–1342.
- Bray, J. D. and Travasarou, T. (2007). Simplified procedure for estimating earthquake-induced deviatoric slope displacements. *J. Geotech. Geoenviron. Eng.*, 133(4), 381–392.
- Harp, E. L. and Jibson, R. W. (1996). Landslides triggered by the 1994 Northridge, California earthquake. *Seismological Society of America*, 86, S319-S332.
- Jibson, R. W. (2007). Regression models for estimating coseismic landslide displacement. *Engineering Geology*, 91(2007), 209-218.
- Jibson, R. W. and Michael, J. A. (2009). Maps showing seismic landslide hazards in Anchorage, Alaska: U.S. Geological Survey Scientific Investigations Map 3077, scale 1:25,000, 11-p. pamphlet. [Available at URL <http://pubs.usgs.gov/sim/3077>]
- Jibson, R. W., Harp, E. L., and Michael, J. A. (2000). A method for producing digital probabilistic seismic landslide hazard maps. *Engineering Geology*, 58(2000), 271-289.
- Kanno, T., Narita, A., Morikawa, N., Fujiwara, H., and Fukushima, Y. (2006). A new attenuation relation for strong ground motion in Japan based on recorded data. *Bulletin of the Seismological Society of America*, 96(3), 879–897.
- Keefer, D. K. (1984). Landslides caused by earthquakes. *Geological Society of America Bulletin*, 95.
- Keefer, D. K. (2002). Investigating landslides caused by earthquakes - a historical review. *Surveys in Geophysics*, 23, 473-510.
- Kieffer, D. S., Jibson, R. W., Rathje, E. M. and Kelson, K. (2006). Landslides triggered by the 2004 Niigata Ken Chuetsu, Japan, Earthquake. *Earthquake Spectra*, 22(S1), S47–S73.
- Moran, E. H. and Galloway, D. L. (2006). Ground-water in the Anchorage area, Alaska - meeting the challenges of ground-water sustainability. U.S. Geological Survey Fact Sheet 2006-3148.
- Newmark, N. (1965). Effects of earthquakes on dams and embankments. *Geotechnique*, 15(2), 139-160.
- Parise, M. and Jibson, R. W. (2000). A seismic landslide susceptibility rating of geologic units based on analysis of characteristics of landslides triggered by the 17 January, 1994 Northridge, California earthquake. *Engineering Geology*, 58(2000), 251–270.
- Petersen, M. D., Frankel, A. D., Harmsen, S. C., Mueller, C. S., Haller, K. M., Wheeler, R. L., Wesson, R. L., Zeng, Y., Boyd, O. S., Perkins, D. M., Luco, N., Field, E. H., Wills, C. J., and Rukstales K.S. (2008). Documentation for the 2008 Update of the United States National Seismic Hazard Maps. U.S. Geological Survey Open-File Report 2008-1128.

- Phoon, K. K. and Kulhawy, F. H. (1999). Characterization of geotechnical variability. *Can. Geotech. J.*, 36, 612–624.
- Rathje, E. M. and Saygili, G. (2008). Probabilistic seismic hazard analysis for the sliding displacement of slopes: scalar and vector approaches. *J. Geotech. Geoenviron. Eng., ASCE*, 134(6), 804-814.
- Rathje, E. M. and Saygili, G. (2009). Probabilistic assessment of earthquake-induced sliding displacements of natural slopes. *Bulletin of the New Zealand Society for Earthquake Engineering*, 42(1), 18-27.
- Rathje, E. M. and Saygili, G. (2011). Estimating fully probabilistic seismic sliding displacements of slopes from a pseudoprobabilistic approach. *J. Geotech. Geoenviron. Eng.*, 137(3), 208–217.
- Saygili, G. and Rathje, E. M. (2008). Empirical predictive models for earthquake-Induced sliding displacements of slopes. *J. Geotech. Geoenviron. Eng.*, 134(6), 790–803.
- Saygili, G. and Rathje, E. M. (2009). Probabilistically based seismic landslide hazard maps: An application in Southern California. *Engineering Geology*, 109(2009), 183-194.
- Schmoll, H. R. and Dobrovolny, E. (1972). Generalized geologic map of Anchorage and vicinity, Alaska. U.S. Geological Survey Miscellaneous Investigation Map I-787-A, scale 1:24,000.
- Wesson, R. L., Boyd, O. S., Mueller, C. S., Bufe, C. G., Frankel, A. D., and Petersen, M. D. (2007). Revision of time-independent probabilistic seismic hazard maps for Alaska. U.S. Geological Survey Open-File Report 2007-1043, 41 p.
- Wesson, R. L., Frankel, A. D., Mueller, C. S., and Harmsen, S., (1999), Probabilistic seismic hazard maps of Alaska. U.S. Geological Survey Open-File Report 99–36, 43 p.
- Wilson, R. C. and Keefer, D. K. (1985). Predicting areal limits of earthquake-induced landsliding. in *Evaluating Earthquake Hazards in Los Angeles Region*, Zinoy, J.L., ed., U.S. Geological Survey, Reston, Virginia, Professional Paper 1360, 317-345.
- Wilson, R. C., Keefer, D. K. (1983). Dynamic analysis of a slope failure from the 6 August 1979 Coyote Lake, California, earthquake. *Bulletin of Seismological Society of America*, 73, 863–877.
- Yahle, L. A., Schmoll, H. R., and Dobrovolny, E. (1992). Surficial geologic map of the Anchorage A-8 SE quadrangle, Alaska. U.S. Geological Survey Open-File Report 92-350, scale 1:25,000.
- Youngs, R. R., Chiou, S. J., Silva, W. J., and Humphrey, J. R., (1997). Strong ground-motion attenuation relationships for subduction zone earthquakes. *Seismological Research Letters*, 68(1), 58–73.